THESIS

REAL-TIME MODELING AND SIMULATION OF DISTRIBUTION FEEDER AND DISTRIBUTED RESOURCES

Submitted by

Pawan Singh

Department of Electrical and Computer Engineering

In partial fulfillment of the requirements

For the Degree of Master of Science

Colorado State University

Fort Collins, Colorado

Fall 2015

Master's Committee:

Advisor: Siddharth Suryanarayanan

Sudipta Chakraborty
Dan Zimmerle

ABSTRACT

REAL-TIME MODELING AND SIMULATION OF DISTRIBUTION FEEDER AND DISTRIBUTED RESOURCES

The analysis of the electrical system dates back to the days when analog network analyzers were used. With the advent of digital computers, many programs were written for power-flow and short circuit analysis for the improvement of the electrical system. Real-time computer simulations can answer many what-if scenarios in the existing or the proposed power system. In this thesis, the standard IEEE 13-Node distribution feeder is developed and validated on a real-time platform OPAL-RT^{TM}. The concept and the challenges of the real-time simulation are studied and addressed. Distributed energy resources includes some of the commonly used distributed generation and storage devices like diesel engine, solar photovoltaic array, and battery storage system are modeled and simulated on a real-time platform. A microgrid encompasses a portion of an electric power distribution which is located downstream of the distribution substation. Normally, the microgrid operates in paralleled mode with the grid; however, scheduled or forced isolation can take place. In such conditions, the microgrid must have the ability to operate stably and autonomously. The microgrid can operate in grid connected and islanded mode, both the operating modes are studied in the last chapter. Towards the end, a simple microgrid controller modeled and simulated on the real-time platform is developed for energy management and protection for the microgrid.

ACKNOWLEDGEMENTS

This thesis was possible by the help, guidance, and support of many people. I would like to thank my advisor, Dr. Siddharth Suryanarayanan and Dr. Sudipta Chakraborty for the guidance and wisdom they provided throughout my time at Colorado State University and National Renewable Energy Lab. Thank you also to Dr. Dan Zimmerle for agreeing to be a part of my thesis committee.

I would especially like to thank Austin Nelson for helping and guiding me throughout the project at National Renewable Energy Laboratory. I would also like to thank the Jerry Duggan and OPALRT™ technical support team for the advice and suggestions which were extremely helpful to operate OPAL-RT™ at Colorado State University. Lastly I would like thank my family and friends for their unwavering love and support.

TABLE OF CONTENTS

LIST OF TABLES

LIST OF FIGURES

Chapter 1

INTRODUCTION

1.1 BACKGROUND

The modernized electricity grid, often termed as the Smart Grid, is a complex cyber-physical entity in which classical power system technologies are intertwined with emerging advances in technologies related to renewable energy sources, distributed resources, power electronics, controllable loads, sophisticated control system, diverse communication mediums and protocols, and active end-users enabled with forecast and near real-time information. The distribution realm of the electricity grid is seeing unprecedented modernization with the advent of the above mentioned technologies [1]. A representative concept of the Smart Grid is the microgrid, a self-containing subset of an area electric power system operating at distribution voltages with access to loads, controls and protection, and multiple sources of generation. Further, the microgrid presents itself as a single unit of control to the utility grid, from which it may be intentionally islanded for operation [2].

The interactions between the various component assets and the system in a complex cyber-physical realm may require comprehensive studies for full characterization of the critical infrastructure, i.e., the electricity grid. Test platforms for performing both real-time (RT) and hardware-in-the-loop (HIL) experiments enable such studies. The former is a fast digital simulation technique of time steps in the order of a few microseconds for quantifying steady-state, dynamic, and transient characteristics over long (realistic) horizons of simulation. The latter is an experimental technique where an actual hardware is included in the simulation loop for characterization. The

high fidelity of the simulations will make the hardware under test oblivious to the lab environment by mimicking reality- while not compromising on the grid-side complexity of the test procedure. The hardware can be tested, characterized, and validated for standard compliance, system-level operation, interoperability, functional specification, and communication variations.

In that regard, the Energy Systems Integration Facility (ESIF) of the National Renewable Energy Laboratory (NREL) and collaborators from Colorado State University (CSU) designed and developed a flexible cyber-physical platform for testing electric power microgrids. In this test platform, actual hardware interfaces with a system or network-level abstractions of the electric grid while maintaining the fidelity of the latter using sophisticated simulation models. In addition to testing hardware assets in a RT and HIL environment, the setup is capable of tests on different communication phenomena (e.g., protocols, latency and bandwidth requirements), loss of package, cyber-attacks, and data management. The effort of the personnel from Advanced Power Engineering Laboratory (APEL) of CSU in developing the testbed at NREL relates to the following: a) development of real-time models of renewable generation, loads, electrical storage, and power electronics; and, b) development of the electrical backbone model for the microgrid system, i.e., the distribution grid.

This report details procedure, challenges and solutions, and results pertaining to the modeling and simulation of the IEEE 13-Node distribution network and distributed resources including a diesel engine, a solar photovoltaic array, and battery storage models on a real-time platform, i.e., OPAL-RT^{TM}. These simulations can be performed using a real-time simulator from OPAL-RT^{TM}. The system can be used for controlling kW to MW scale power equipment, thus creating realistic test platforms to conduct integration testing at actual power and load levels to evaluate component and system performance before commercialization [3].

1.2 LITERATURE REVIEW

Digital real-time simulator has been used for many years in power system sector; and there are many commercial simulators have been developed based on Dommel's algorithm implemented in EMTP simulation program [4]. The OPAL-RT^{TM} real-time simulator based on the user-friendly commercial product consists of ARTEMIS and RT-LAB. Testing of complex HVDC networks, SVCs, STATCOMs and FACTS device control systems, under steady state and transient operating conditions, is a mandatory practice during both the controller development phase and before final system commissioning [5]-[6].

The integration of DG devices, including some microgrid applications, and renewable energy sources (RES), such as wind farms, is one of the primary challenges facing electrical engineers today [7]-[8]. It requires in-depth analysis and the contributions of many engineers from different specialized fields. According to IEEE std. 1547-2003, intentional or planned islanding is still under consideration by many utilities [9]-[10]. The Consortium for Electric Reliability Technology Solutions (CERTS) executive summary report in [11] presents the results of ongoing investigations on development of high power electronic systems for distributed generation systems using standardized approaches for integrating the components that comprise power converters.

The balance between supply and demand of power is an important requirement of microgrid in both the islanded and the grid connected mode. In grid connected mode the power requirement is met by exchanging the power with the grid. [12], [13]. Microgrid technologies such as energy management, protection control, power quality, and field test have been studied. A distributed intelligent energy management was developed in [13], [14]. Pilot plants for microgrid have been developed and tested using emulated laboratory microgrid [15]. Demonstration and pilot projects for demonstration and testing of microgrid [15]-[21]. Field tests for frequency and voltage control, and utility interconnection devices [15]-[17]. Hardware in loop technologies are has been used in various engineering technologies such as power electronics, robotics, and automotive system.

[22]-[24]. Real time digital simulator (RTDS) is a special purpose computer designed to study the electromagnetic transients in real-time. RTDS utilizes the advanced parallel processing technique. RTDS have been used for testing of high voltage direct current, static var compensators, and protective relays [25]-[31].

During literature survey on the aspects of integration of DERs it is further revealed that the latest technological development in this field of research, in recent years, is aimed at the maximum utilization of various types of renewable energy sources (RESs) due to great advantage of abundance availability and less environment impact.

1.3 OBJECTIVES AND OUTLINE

The main objective of this study is to develop a real-time model of a distribution system for HIL study. The model should be validated and quantified on a real-time platform. The study should present the challenges encountered and the solution to those challenges. The distributed resources should be selected and modeled in a real-time platform and, these models will form the microgrid with the 13-Node distribution system. The other important aspect of the microgrid is the microgrid controller which should be developed and tested under different scenarios.

All the chapters in this thesis starts with an brief introduction to the contents presented in the chapter and end with a summary and next steps towards the objective. Chapter 2 contains the information regarding modeling of the 13-Node distribution system. It explains all the modeling aspects of the 13-Node distribution system in Simulink. Various types of load and line configurations are explained in detail. Chapter 3 explains the real-time modeling of the 13-Node distribution system and explains the real-time simulator OPAL-RT^{TM}. This chapter also deals with the concept of multi-core simulation and why it is necessary to take this approach. Finally the model is validated in real-time with an acceptable accuracy. Chapter 4 deals with the development of distributed resources such as diesel generator, photovoltaic system, and battery inverter system.

These models are validated in real-time simulation and these forms the basis of the microgrid. The microgrid formed is simulated in real-time with all the distributed resources developed in this chapter. Chapter 5 models a microgrid controller which has the capability to control the battery system to compensate for step changes in loads and variation in photovoltaic system. The developed microgrid is simulated for various scenarios of the microgrid operation and then simulation results are discussed along with the waveforms. Finally, a conclusion for the thesis and future work are suggested and discussed in chapter 6.

Chapter 2

MODELING THE IEEE 13-NODE DISTRIBUTION FEEDER

2.1 INTRODUCTION

Many computer programs are available for analysis of distribution feeders. A paper [34] was published to make the data for radial distribution feeder available to program developers and to verify the correctness of the computer simulation results. Many computer programs are available for the analysis of unbalanced three phase radial distribution feeder. There was a need to benchmark the test feeder to obtain comparable results from various computer simulators. The complete data and solutions for all of the test feeders can be downloaded from the Internet at [35] While the literature on the distribution system is abundant [32]-[35], the use of real-time simulation for these simulation is lacking.

The primary objective of this work includes selection, validation, and modeling of a distribution feeder in Simulink™ and RT-LAB™, followed by validating the model in a real-time simulator OPAL-RT™. The model will be used in PHIL simulations for forming a microgrid with photovoltaic and battery inverter system as the actual power hardware in the loop.

2.1.1 THE IEEE 13-NODE TEST FEEDER

The reason for choosing the IEEE 13-Node test feeder model was the interesting characteristics exhibited by this distribution feeder, which are listed as follows:

1. The 13-Node test feeder is relatively short (8200 ft) and highly loaded for a 4.16 kV feeder. The longest line is 2000 ft long.

2. There is one substation voltage-regulator consisting of three single-phase units connected in wye. This regulator has capability to change secondary voltage in steps of 0.00625 per-unit (pu).

3. There are overhead and underground lines with variety of phasing in this feeder.

4. There are two shunt capacitor banks. One at node-675 with 200 kVAr each phase and the other one at node-611 with 100 kVAr.

5. There is one in-line transformer between node-633 to node-634. The transformer is 500kVA 4.16 kV/ 480 V in wye-ground configuration.

6. There are unbalanced spot and distributed loads, which are of Constant PQ, I, or Z type connected in delta or wye configuration.

One of the other reasons for selecting this test feeder is that, it is verifiable from the available test data and it is relatively smaller with 13 electrical nodes making it conducive to simulate on a reasonably sized real-time platform. Figure 2.1 shows single line diagram for 13-Node distribution model.

2.1.2 MODELING THE IEEE 13-NODE TEST FEEDER IN SIMULINK^{TM} / SIMPOWERSYSTEM^{TM}

TOOLS AND TECHNIQUE

Simulink^{TM} [36] is a block diagram environment for multi-domain simulation and model-based design. It supports simulation, automatic code generation, and continuous test and verification of embedded systems.

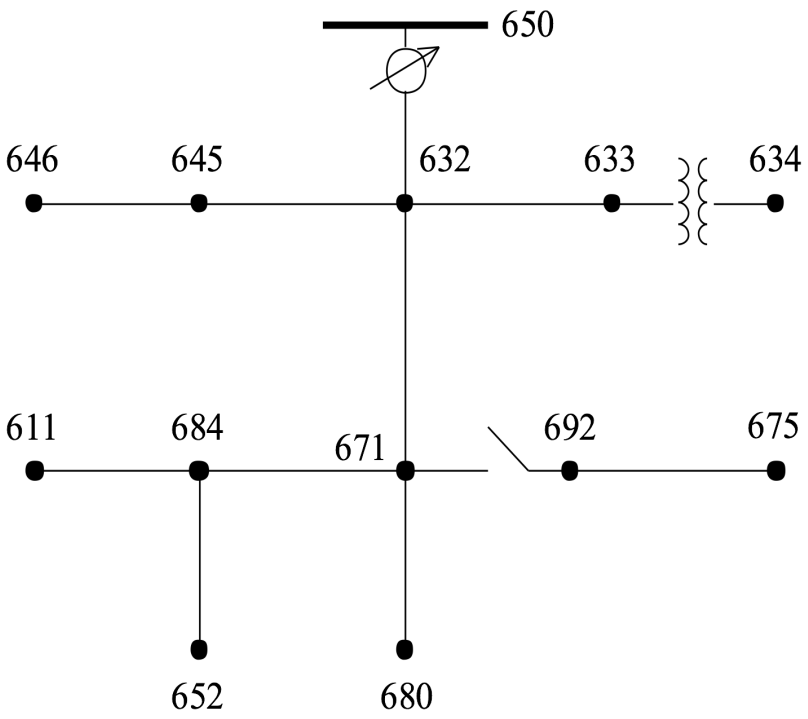

Figure 2.1: The IEEE 13-Node test feeder.

Simulink™ provides a graphical editor, customizable block libraries, and solvers for modeling and simulating dynamic systems. It is integrated with MATLAB™, enabling you to incorporate MATLAB™ algorithms into models and export simulation results to MATLAB™ for further analysis. Appendix-A.1 gives the versions and Simulink™ toolbox available for modeling.

Some of the basic electrical components are available under the Simulink™ library and these component serve as building block for the model. Examples and demo models in Simulink™ [36] served as the basis for development of some components in the distribution feeder model. The following subsection describe the modeling and parameter selection for the developed Simulink™ models.

LOAD MODEL

The IEEE 13-Node distribution feeder consists of three phase or single phase constant PQ, I, or Z load connected in delta or wye configuration. The three phase balanced load can be modeled by

using a three phase dynamic load which is available under the SimPowerSystem™ library. The load real power P (W) and reactive power Q (vars) is given by equation (2.1) and (2.2) [37]:

$$P = P_0 \left(\frac{V}{V_0} \right)^{n_p} \tag{2.1}$$

$$Q = Q_0 \left(\frac{V}{V_0} \right)^{n_q} \tag{2.2}$$

where,

P_0 and Q_0 are the initial active and reactive power at the initial Voltage V_0

n_p and n_q are constants controlling the nature of load i.e., constant PQ, I, or Z

The 13-Node distribution model requires unbalanced load models, which is modeled using a single phase dynamic load block given in Simulink™ example[38]. The delta connected load rating for Phase-A, Phase-B and Phase-C refer to the ratings of the loads connected between phases A-B, B-C and C-A respectively. If not specified, the neutral is grounded by default. By setting the parameter [n_p n_q] in Simulink™ block as 0, 1, or 2 for constant PQ, I, and Z load, respectively, the desired load configuration can be obtained. Figure 2.2 shows the parameters in the Simulink™ block for load configuration according to the IEEE 13-Node test data. The parameters shown are for the load at node-692, which is D-I configuration and the load is 170 kW and 151 kVAr at phase-C. This delta load is connected between phase C-A. If a single phase load is wye configuration then it is connected between line to ground. Parameters [n_p n_q] are set as 1 for constant I type load and the nominal voltage is set to 4.16 kV for phase-phase connection.

DISTRIBUTION FEEDER LINE MODEL

There were several options available for the line model such as ARTEMIS Distributed Parameter Line (DPL), PI-line model in Simulink™. ARTEMIS DPL can be used in the model as it has a major advantage of decoupling both side of the line into 2 distinct state-space systems and to make

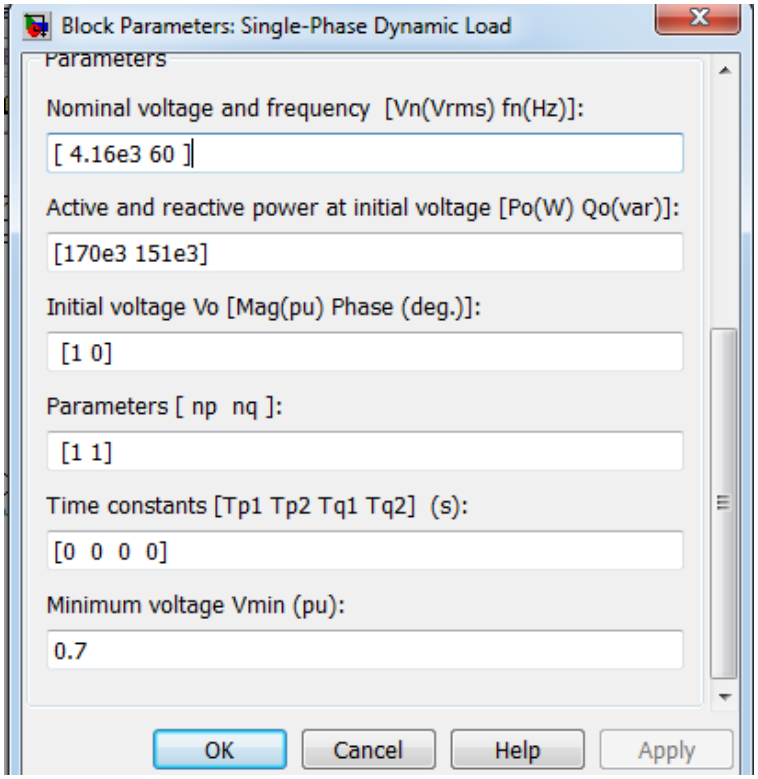

Figure 2.2: Simulink™ dynamic load model parameters.

the overall simulation much faster. The ARTEMIS DPL model has the limitation that a sufficient natural propagation delay must exist in the model. With the speed of light being 300000 km/s, the minimum line length is related to the sample time of the model given by (2.3)

$$Length_{min} = \frac{T_s}{3.3 \times 10^{-6}} \tag{2.3}$$

where, $Length_{min}$ is the minimum line length in km and Ts is the model sample time or step size in seconds.

Using this equation with Ts = 50 μs the minimum length is calculated as 15 km for the DPL. For modeling that requires smaller lengths stub-line can be used, which allow time delay between subsystems to be at least 1 time step. In the 13-Node distribution model, the longest line length is 2000 ft or 0.61 km thus this method cannot be used because of the low propagation time.

The IEEE 13-Node distribution system has unbalanced three-phase load and the line parameters are given in impedance and admittance matrix data. Hence, a PI-line model was developed in Simulink™ with R-L in parallel with C/2 at each end using the RLC model branch [41] model in Simulink™ as shown in Figure 2.3. This matrix element represents G+jB, where G was negligible. The line capacitance C is calculated as $C = \frac{B}{2\pi f}$. R, L and B line parameters were obtained from the feeder test data.

$$z = R + j\omega L = R + jX$$

$$y = \frac{1}{R_{sh}} + j\omega C = G + jB$$

Where R is the series resistance (Ω/m), X is the series reactance (Ω/m), G is the shunt conductance (S/m), and B is the shunt susceptance (S/m)

The IEEE 13-Node distribution feeder test data provide data for impedance and admittance matrix [35]. A MATLAB™ script written to parameterize the line data is given in appendix-A.2. The line model parameters R, L, and C are specified according to the type of line, the nomenclature for line parameters is: **Parameter_Type of line**, usage is given in Appendix-A.1. For a line type-601 [35] the resistance, inductance, and capacitance will be given by R_601, L_601 and C_601 respectively.

VOLTAGE REGULATOR

A step-voltage regulator consists of an autotransformer and a load tap changing mechanism. A standard step regulator contains a reversing switch enabling $\pm 10\%$ regulator usually in 32 steps, which amount to 5/8% change in voltage. A common type of step voltage regulator is type-B as given in [40].

The Simulink™ model for OLTC is available under Simulink™ library is a phasor model. De-

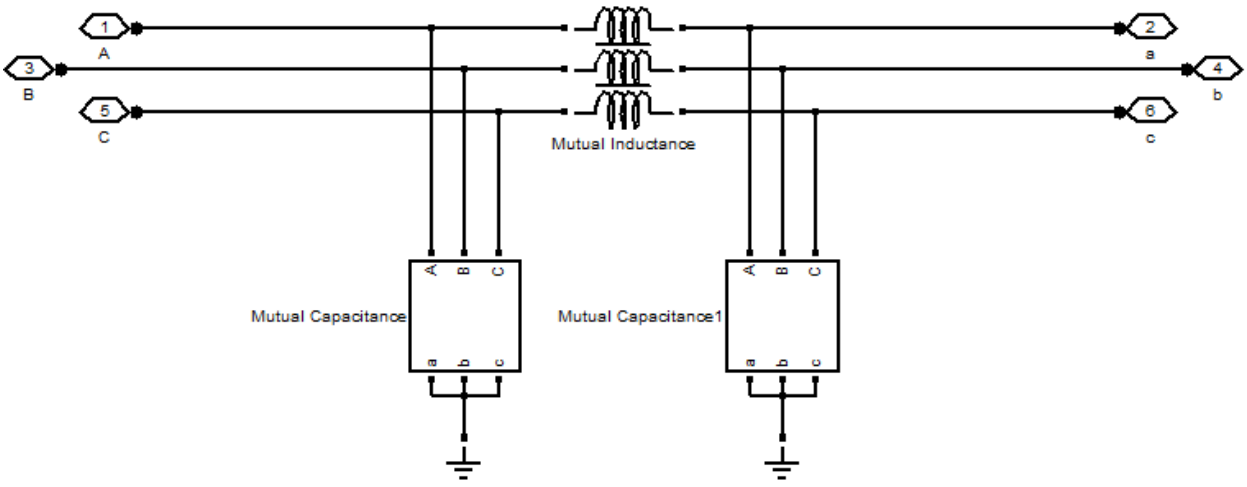

Figure 2.3: 3-phase PI line model.

tailed model of the OLTC is obtained from the Simulink™ example: **power_OLTCregtransformer**. To make this model compatible with 13-Node distribution test data following changes were made to the OTLC model in Simulink™.

1. The model given in Simulink™ example consists of only 18 taps, but the IEEE 13-Node distribution model requires 32 steps or ± 16 steps. The procedure to change the number of taps in the model is given in Appendix-A.3.

2. The 13-Node distribution model is an unbalanced feeder, which requires an independent control for tap changing mechanism. The control was modified by making the control available for one tap changing mechanism was modified by replicating the tap changing control for all the three phases.

3. Per-unit voltage change for one step change is 0.00625 pu We need a regulation between 0.9 pu -1.1 p.u with ± 16 steps. One step change will be: $\frac{0.2}{32} = 0.00625pu$

4. The transformer voltage level changed to 115 kV for the primary and 4.16 kV for the secondary.

The on-line tap changer (OLTC) transformer model given in the Simulink™ library is not capable of changing the tap of each phase individually [39]. Taps are changed according to the measured pu voltage, assuming a balanced 3-phase system but, the 13-Node distribution system is an unbalanced system. The control system for the Simulink™ library model of the tap changer was modified to change the tap of each phase of the 3-phase autotransformer individually by using the same tap changing control for each of the phases. Standard tap changing transformers have a reversing switch enabling 10% regulator range in 32 steps, resulting in 0.625% per step change [8]. These values are specified in the Simulink™ model parameters. The pu transformer reactance and resistance values are specified as referred to the second winding of the autotransformer. The leakage reactance of the OLTC transformer was varied and the pu voltages were recorded which is shown in Figure 2.4. This is similar to what is expected, as obtained in [42].

VERIFICATION

The new model was verified by changing the tap of the OLTC transformer and recording the output pu voltage. Figure 2.5 shows Phase-A, Phase-B and Phase-C changing pu values in 0.0625 pu steps as the taps of OLTC are changing. This verifies that OLTC is woking correctly and changing steps as per the desired control.

TRANSFORMER, BREAKER, AND CAPACITOR BANK

3-phase transformer and breaker models were obtained from SimPowerSystems™ library in Simulink™. The values of voltages, nominal transformer power, and the pu reactances and resistances were obtained from the IEEE 13-Node test system data [35]. Capacitor banks were modeled using a series RLC load branch from the SimPowerSystems™ library in Simulink™ as shown in Figure 2.6. QL and P were set to zero as shown in Figure 2.7, where V is line-line voltage and Qc is the reactive power of the capacitor bank in VAr. The capacitors were connected in star or grounded configuration and the respective KVAr values were obtained from the IEEE 13-Node test system.

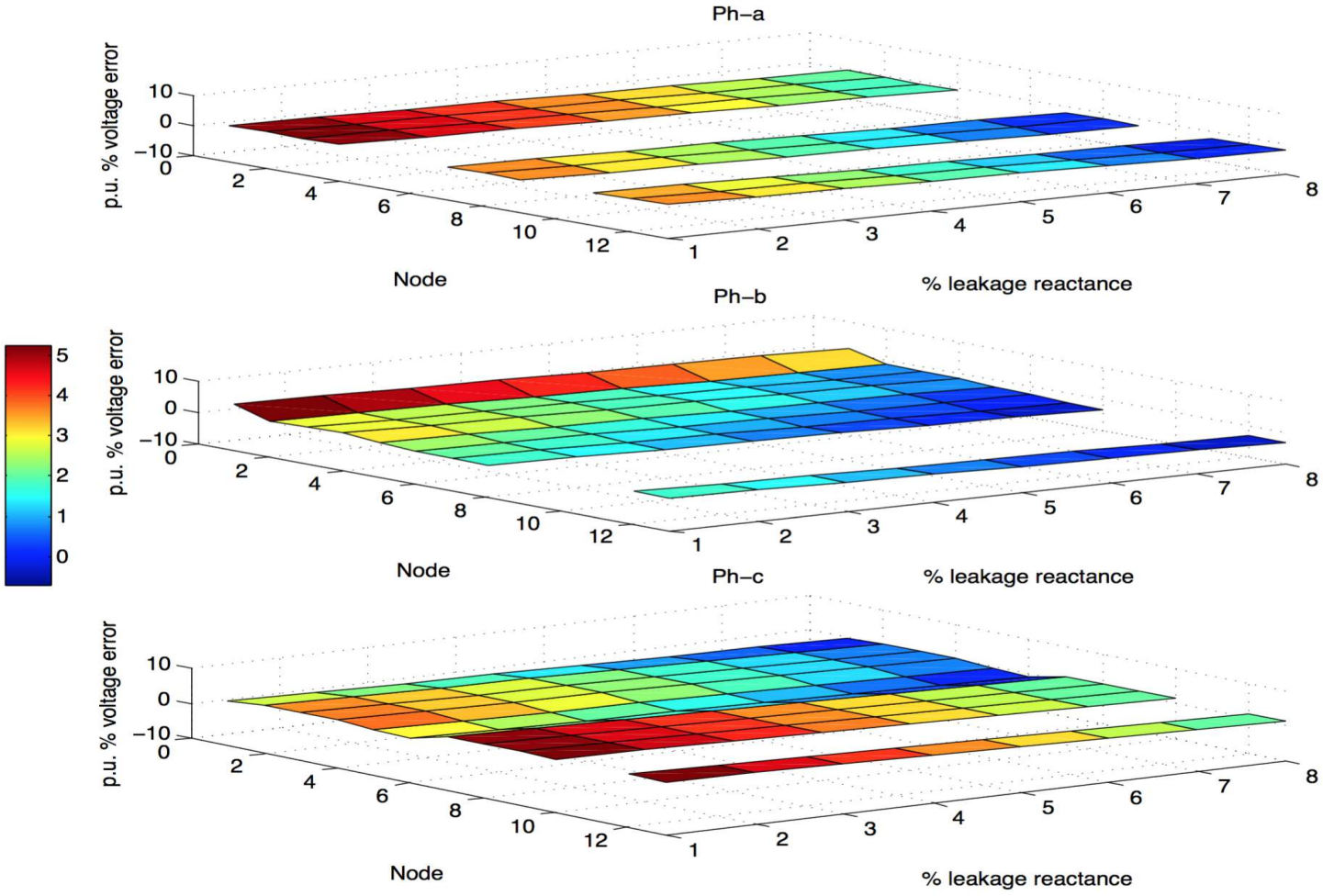

Figure 2.4: Pu voltage variation with change in leakage reactance of the OLTC.

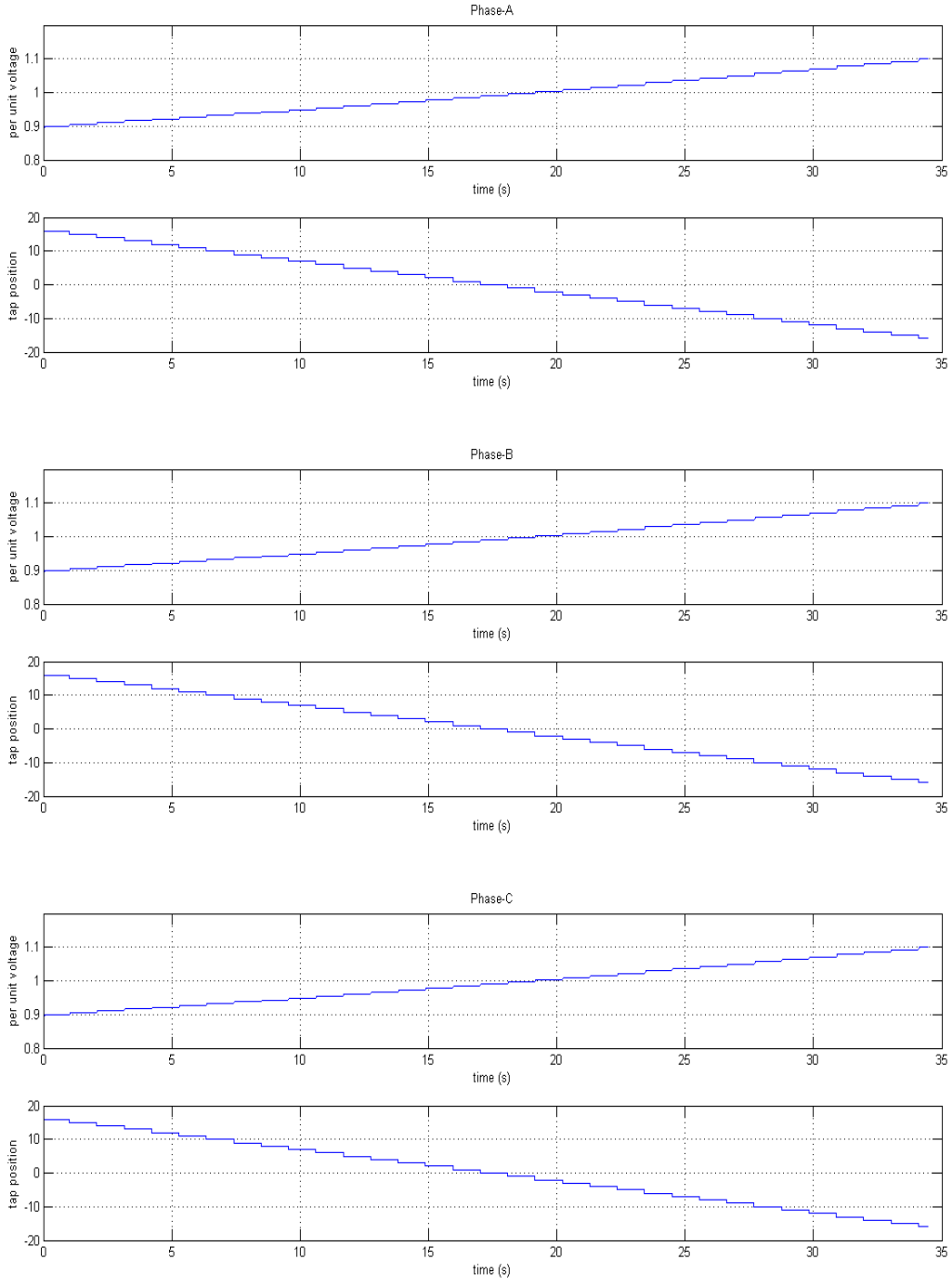

Figure 2.5: OLTC transformer test with change in pu voltage with changes in steps.

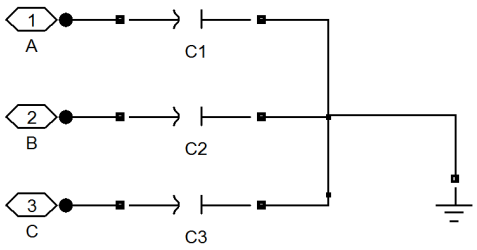

Figure 2.6: 3-Phase capacitor bank model in Simulink™.

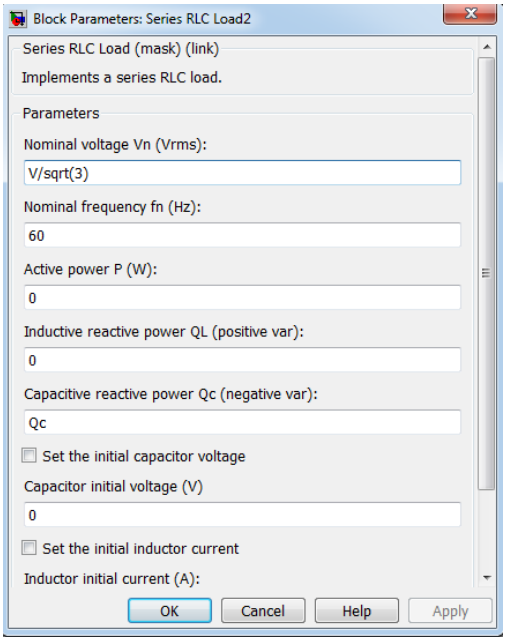

Figure 2.7: Simulink™ model parameters for capacitor bank model.

Chapter 3

REAL-TIME MODELING IN OPAL-RT™

3.1 INTRODUCTION

A discrete-time constant step duration simulation is assumed for discussion in this thesis. Discrete time simulation means that time moves forward in fixed step size, which is also known as fixed time step simulation. Even though there are some methods and simulation such as variable step solver in Simulink™, which use variable step size for solving high frequency dynamics, they are unsuitable for real-time simulation [43].

HARDWARE AND SOFTWARE REQUIREMENT FOR MODELING AND SIMULATION

The hardware and software tools used for modeling and simulation in this thesis are given in Table 3.1.

Table 3.1: Hardware and Software requirement

Hardware	Software
OPAL-RT™ OP5600	Host operating system: Windows 7™
12 active cores at 3466 MHz	Target operating system: Redhat™ 2.6.29.6-opalrt-5
i686 architecture	RT LAB™ v10.5.9
	Matlab™ v2011b
	Simulink™ v7.8

3.1.1 TIMING MECHANISM IN OPAL-RT^{TM} AND RT-LAB^{TM}

A real-time simulation is based not only on the computational speed of the hardware, but also on the computer model's complexity. A real-time simulator would produce results at within the same amount as its real world physical model would. The time step is the time required not just for computing the mathematical model, but it also includes the time to drive the input and output (I/O) ports. The idle time of the simulation is lost, i.e., if the computation is finished before the end of time step the remaining time is lost. Figure 3.1 explains this phenomenon in the real-time simulation.

In Figure 3.1, during the time step Ts = 1 and Ts = 2 the computation and I/O is completed within the time step and idle time is lost, the next step is not started until Ts = 3. An overruns occur in a simulation if the cycle of receiving the data, performing computation and sending output is not performed with in the given time step, which is shown in Figure 3.1 at Ts = 3. At time step Ts = 3, the cycle is not completed, this is known as overrun. Because of the overrun in the model the model is frozen for Ts = 4, i.e., no computation is done for the next time step. The time step Ts = 4 is lost and no computation is performed because the last time step Ts = 3 had overrun. Overruns in the simulation must be avoided so that model runs in real time and no data is lost due to overruns.

3.2 RT-LAB^{TM} MODELING

RT-LAB^{TM} is a real-time simulation platform for high-fidelity plant simulation, control system prototyping, and embedded data acquisition and control. The unique distributed processing capability of RT-LAB^{TM} allows to quickly convert the Simulink^{TM} models to high-speed, real-time simulations, over one or more target PC processors.

RT-LAB^{TM} enables models in Simulink^{TM} models to interact with real world enabling the hardware-in-loop (HIL) engineering simulators. RT-LAB^{TM} links the code generated with Simulink^{TM}

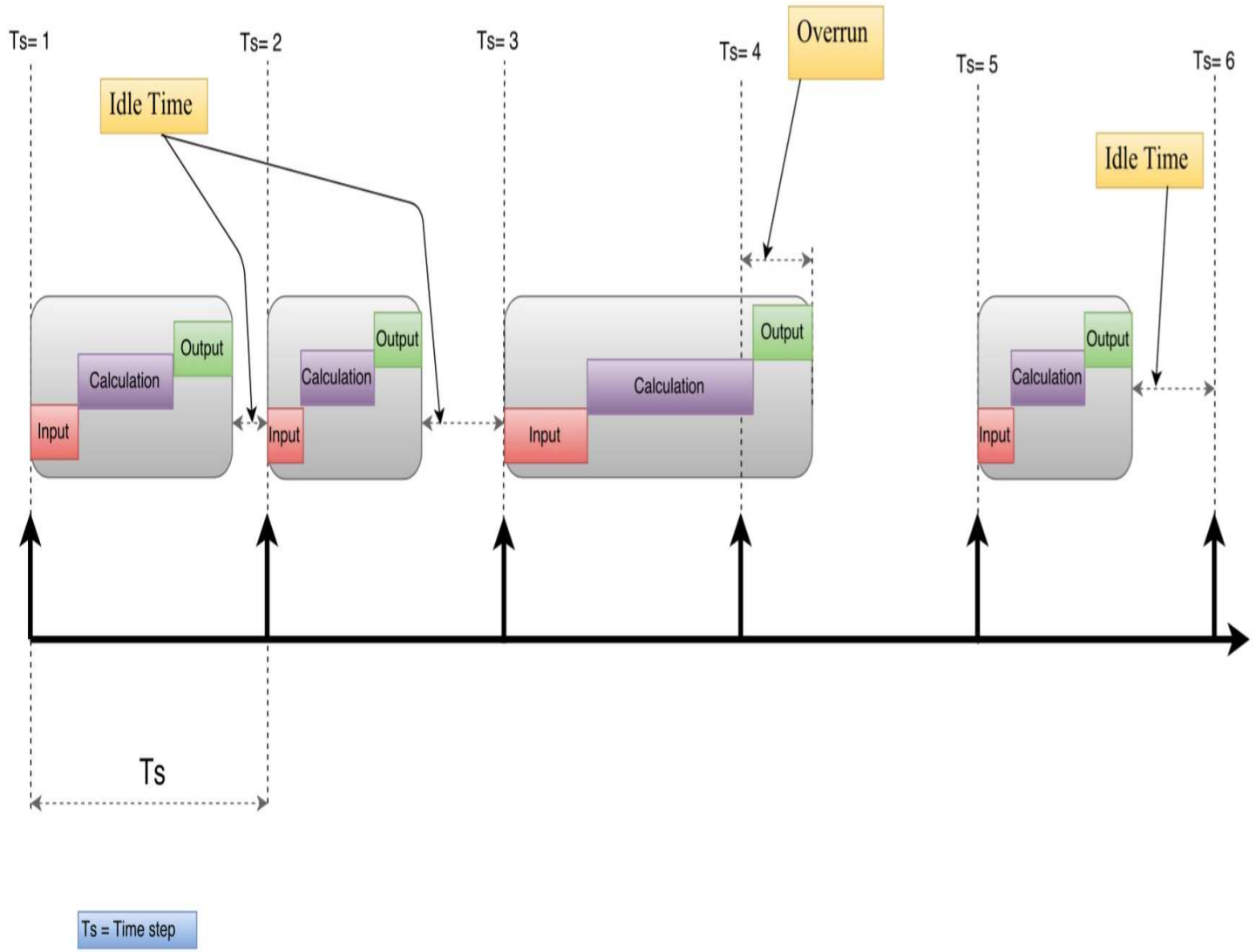

Figure 3.1: RT-LAB^{TM} timing mechanism for time step.

coder to optimized runtime libraries. This helps to achieve a jitter-free fixed step [43]. RT-LAB™ automates the process of preparation, downloading and running of parallel models. There are two parts of OPAL-RT simulator the command station and the target node.

Command station is a Windows™ PC with RT-LAB™ software servers as the development system and user interface. It allows the user to create and prepare the model for distributed real-time execution and interaction during run-time.

Target node is a cluster of PCs where the simulator runs. For a real-time simulation it requires a Real-Time Operating System (RTOS) such as RedHat™ Real-Time Linux. The command station communicates with the target using Ethernet. For HIL simulations, the target communicates with the real world through I/O boards. Each target node can contain one or two processors and each processor can contain one, two, four, or six processor cores.

RT-Model consists of three type of subsystem in the top most level as shown in Figure 3.2 and described in Table 3.2.

A Simulink™ model can be converted into RT-LAB™ compatible model with following changes:

1. Place the ARTEMIS and the POWERGUI blocks at the top most level of the model as shown in Figure 3.2.

2. Place all the scopes in the console subsystem and all the other computational model in the Master subsystem.

3. Use the opcomm block for communication between the subsystems as shown in Figure 3.2. All input ports must go through this block before it is connected inside the subsystem.

Some of the issues, challenges, and solution encountered while modeling in RT-LAB™ are given in appendix-A.6.

Table 3.2: Subsystem properties in RT-LAB™

Subsystem properties in RT-LAB™		
Subsystem	Identifier (Prefix)	Properties
Master	SM_	This subsystem is inaccessible during runtime i.e., no changes can be made during runtime unless a variable is in the console to change it. Every RT-LAB™ model must consists of one of this subsystem.
Slave	SS_	This subsystem is also inaccessible during the simulation, it is an optional subsystem. It is used to split the compute model in multi cores or nodes.
Console	SC_	This is the only subsystem accessible during the runtime, all the scopes and other parameters which needs to be changed and observed during simulation runtime resides here.

Splitting the IEEE the 13-Node Distribution Model

The 13-Node model is placed in master subsystem and simulated in OPAL-RT™, but it had overruns in the model at 50 μs time step. Figure 3.3 shows the CPU usage of the model with varying time step ranging from 50 μs to 225 μs in step of 25 μs. At 50 μs time step the CPU usage is 100%, i.e., the real-time model is running with overruns. Overruns will cause problem in the HIL testing of the model and must be addressed. There are two methods to decouple the system into different core. First method is splitting the model into two cores as given in [44] and the second method is by decoupling the model into multiple core is by using a ARTEMIS DPL line, if the system has line lengths longer than 15 km as discussed in last chapter. Since the lines are shorter the first method of decoupling is chosen.

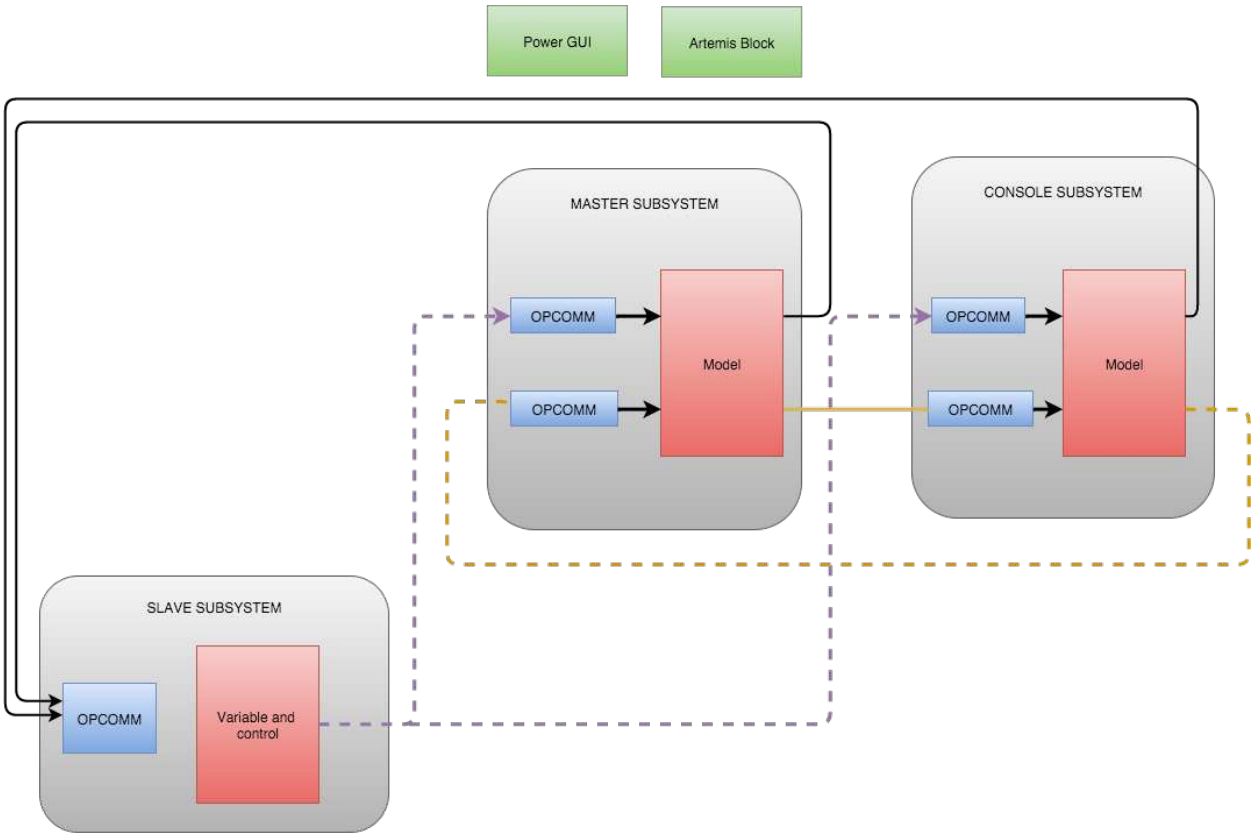

Figure 3.2: Various subsystem in RT-LAB^{TM} model and communication setup.

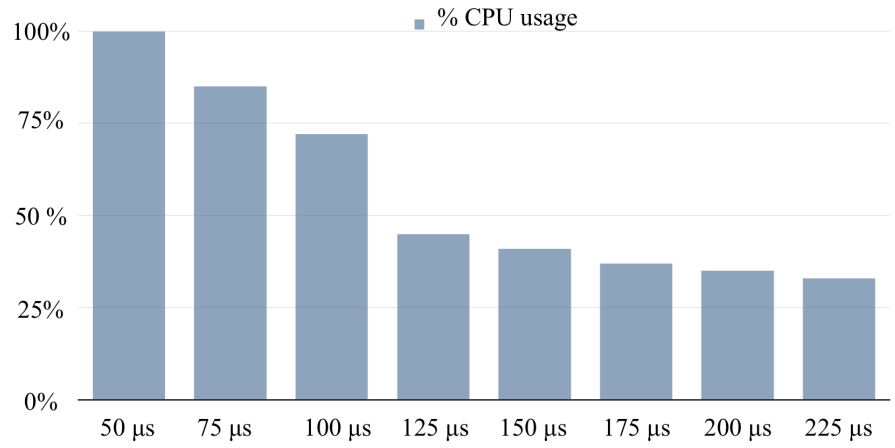

Figure 3.3: CPU usage varying with the time step of the 13-Node distribution model.

Reference [44] gives the method for splitting the model into multiple cores and to reduce the CPU usage in a model. Similar method was used to split the the 13-Node distribution model into 2 cores or computer node as shown in Figure 3.4. The OLTC is placed in master subsystem and all the 13-Nodes are placed in slave subsystem. Output from the OLTC was connected to the current controlled source, which received current signal from the input of the 13-Nodes in slave subsystem. Voltage output form the OLTC in master subsystem, which was input to the controlled voltage source in the slave subsystem was measured. This setup is shown in Figure 3.5

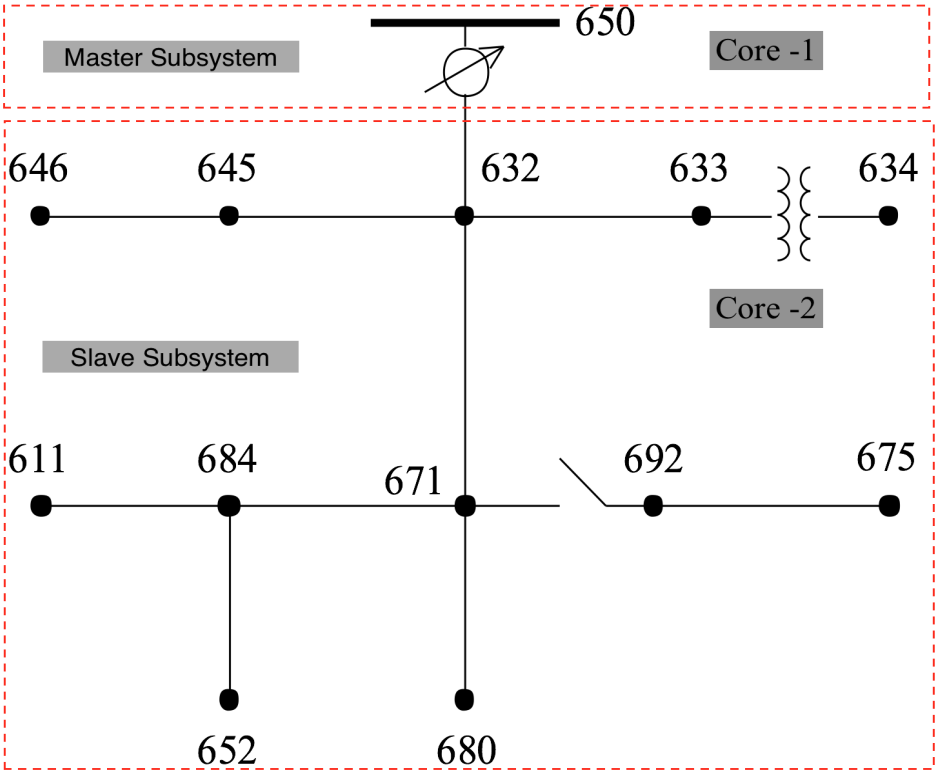

Figure 3.4: Splitting the IEEE 13-Node distribution model in master and slave subsystem.

VALIDATION

The current and voltage waveforms were observed as sine-wave without any disturbance. The pu voltages from the model were recorded and compared with 13-Node test feeder data. After a certain period, the system achieves steady state i.e, when there is no tap changes of the OLTC. The

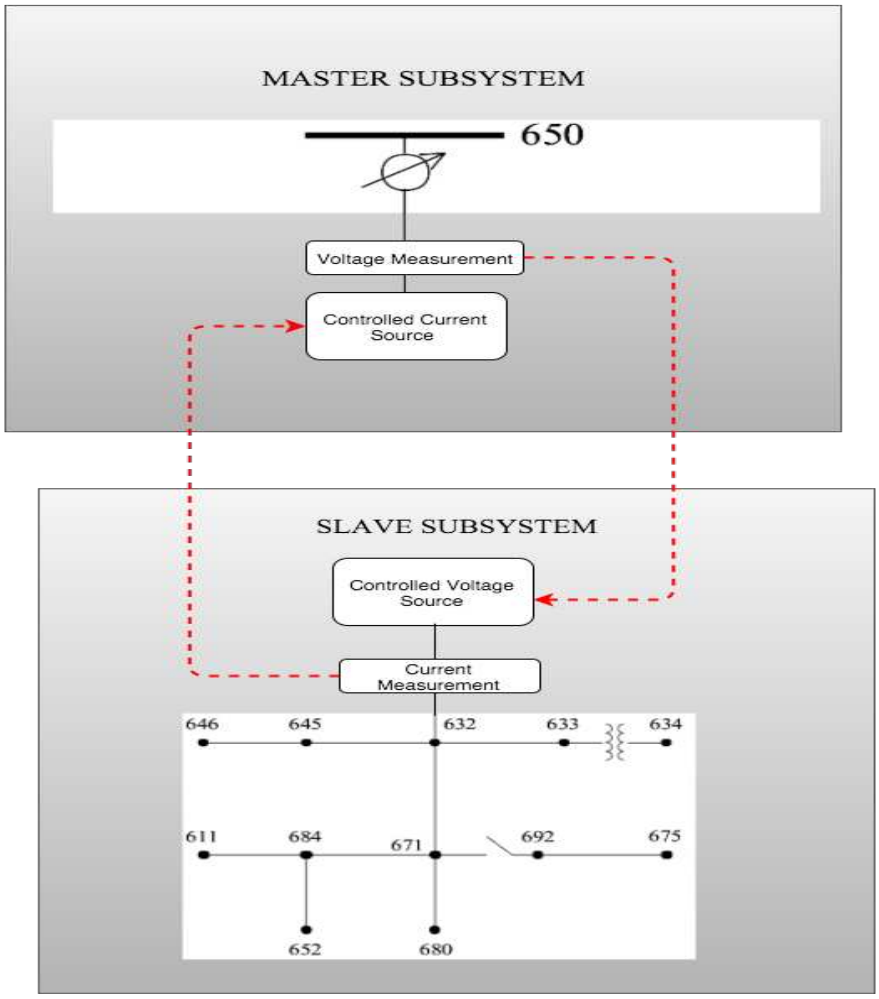

Figure 3.5: The IEEE 13-Node distribution split model.

per unit value of each node voltage is recorded in real-time. These values are used to calculate the percent error at each node using (3.1).

$$error_{rmsvoltage} = \frac{V_{simulation} - V_{ref}}{V_{ref}} \tag{3.1}$$

where, $error_{rmsvoltage}$ is the percentage error, $V_{simulation}$ is the rms voltage at the node from the real-time simulation, and V_{ref} is the rms pu voltage at the node from the IEEE 13-Node test feeder data. Figure 3.6 shows the absolute pu voltage percentage error as compared to the IEEE 13-Node test feeder data, the maximum error is less than 2.5%.

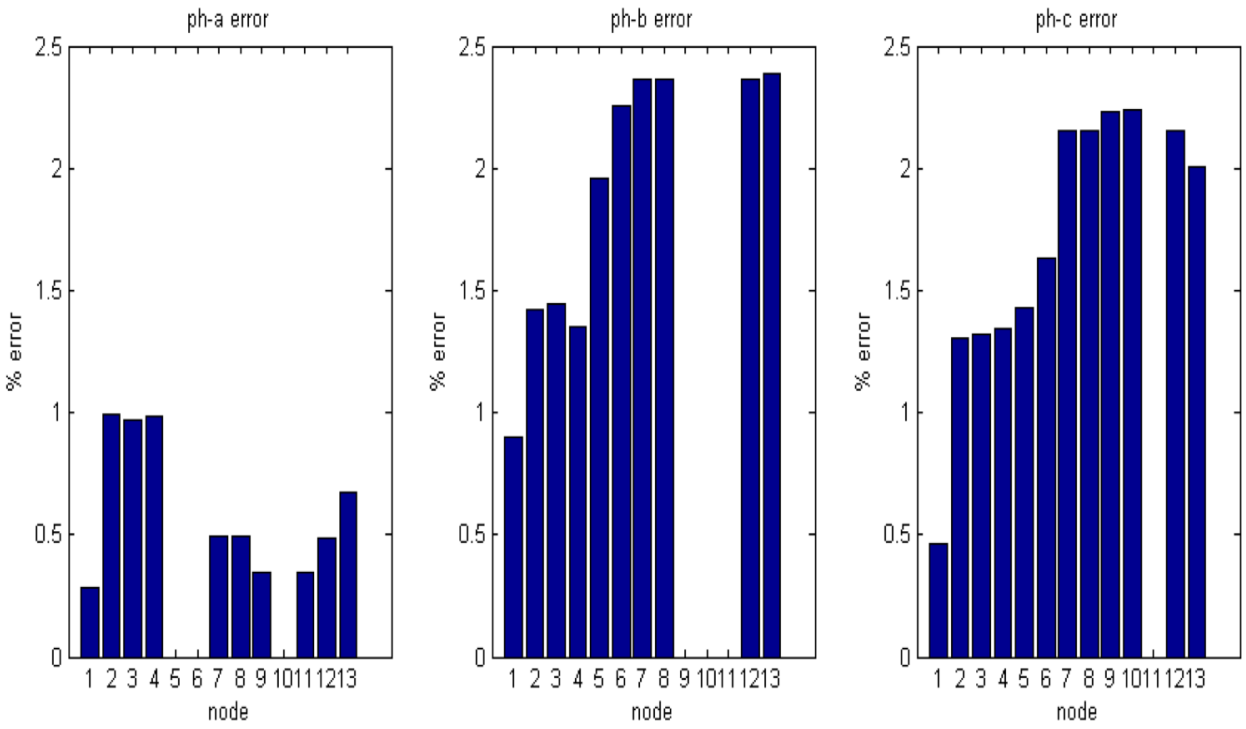

Figure 3.6: Pu absolute voltage percentage error as compared to the 13-Node feeder test data.

3.2.1 ANALOG INPUT-OUTPUT AND PROTECTION

An analog signal is required to drive a real world power hardware. This is obtained from OPAL-RT^{TM} simulation via the use of analog input-output (I/O) board in OPAL-RT^{TM} and I/O blocks in RT-LAB. The analog I/O blocks are available in the Simulink^{TM} library under the RT-LAB^{TM} I/O section. I/O boards on OPAL-RT^{TM} can be configured as follows:

1. Find the right type of I/O port and Board-ID form the RT-LAB^{TM} from “Get I/O info”.

2. Choose appropriate I/O block and connect the multiplexed signal to analog I/O block. Select the voltage range to 5 V, 10V, or 16V as required. If the signal input to the I/O block is greater than specified range the signal will be clipped in the output.

3. Place the OpCtrl block in the model and specify the appropriate Board ID, which can be obtained form the I/O info from RT-LAB^{TM}.

4. Place the bitstream file under the current RT-LAB™ project files.

PROTECTION

The output voltage from the 13-Node distribution feeder is used to drive the grid simulator. A three winding transformer is connected to the secondary side of distribution transformer 4.16 kV/480 V at node-633. The three winding transformer converts the 480 V line-line to 2-phase 3 wire system with 240 V line-line and 120 line-neutral. Figure 3.7 explains the connection of this transformer to the 13-Node distribution system with the I/O and the protection blocks.

The magnitude and frequency of the output voltage is bounded by certain limits, which depends on the input of the grid simulator such as over voltage and over/under frequency. The main concern is not to drive grid simulator with a DC voltage from the 13-Node distribution model.

Phase locked loop block can be used to measure frequency accurately, but it is a more complex block and requires more computation. Hence, a frequency measurement block was modeled in Simulink™. Frequency of a signal can be calculated by counting the number of simulation time steps, 50 μs, between any two zero crossings. The time period can be calculated by multiplying the number of time steps (N) with the fixed step size (Ts). The frequency is given by (3.2).

$$f = \frac{1}{T_s \times N} \tag{3.2}$$

The input voltage is passed through a low pass filter to remove any high high-frequency component in the signal, which might give false zero-crossing trigger. The filtered signal is fed to a custom MATLAB™ function, which detects a zero crossing by observing the change in the sign of the signal.

The MATLAB™ code for zero crossing is given in appendix-A.4. This function outputs a value 1 for every change in sign from negative to positive. This is fed to the counter which counts the number of time steps between these ones, from the zero crossing detector, the code for the

counter is given in appendix-A.4. This values is held and multiplied by the time step to get the period of the wave, reciprocal of this value gives the frequency.

POWER HARDWARE IN THE LOOP (PHIL)

The voltage from the 13-Node distribution model is passed through a gain block to make the voltage level compatible with the grid simulator, which acts as an amplifier. The analog I/O board gives the measured voltages from OPAL-RT^{TM} simulation in the form of analog voltage waveforms. The output current measured from the grid simulator is used to drive the controlled current source in the model. This feedback current and the setup of the microgrid is shown in Figure 3.8. Appendix-A.5 shows the various current level input to the controlled current source with variation in active power and reactive power injected into the distribution system. The pu values of the 480 V/240 V transformer are given with change in current input to the controlled current source.

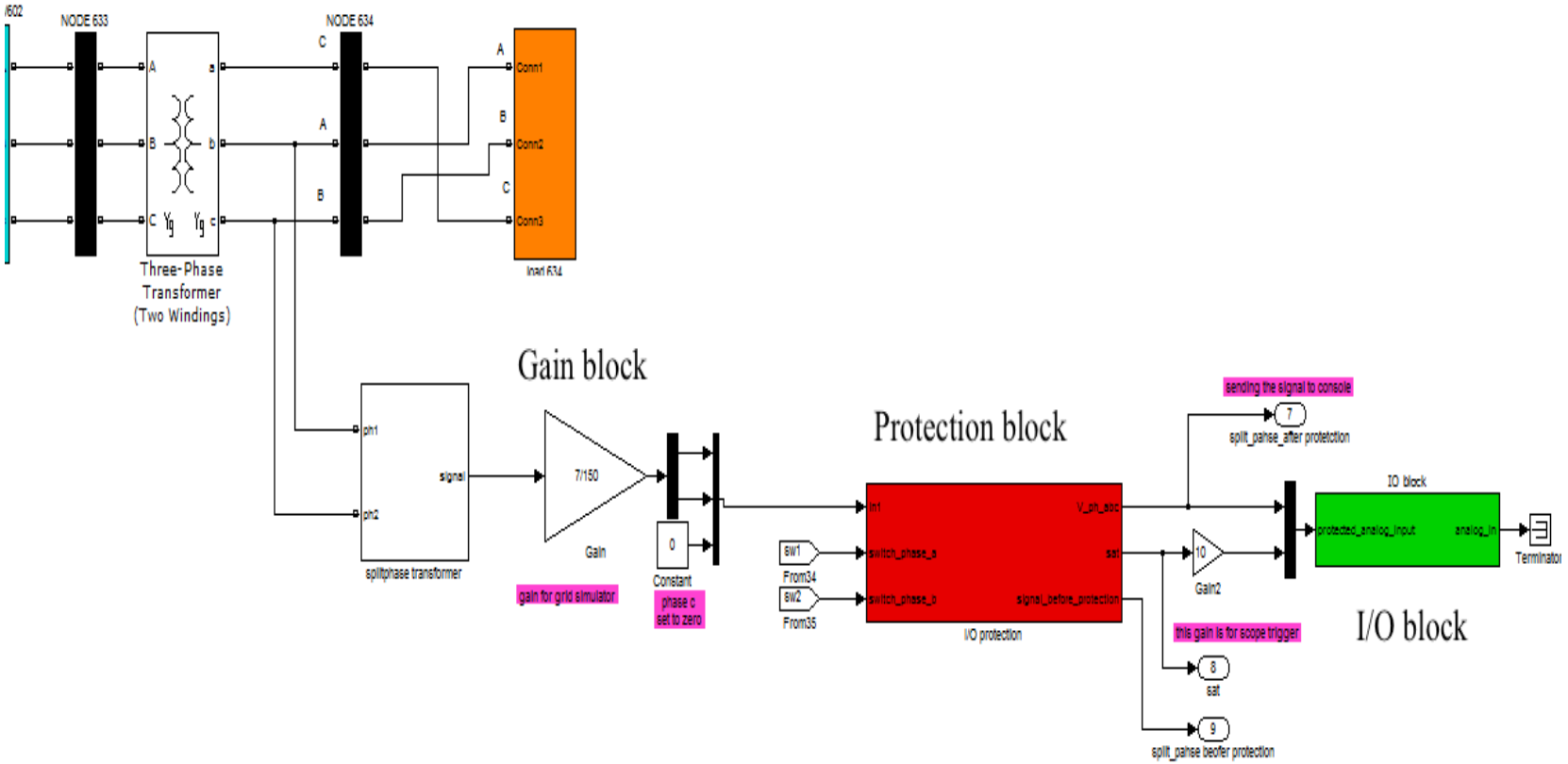

Figure 3.7: Frequency and voltage protection and I/O blocks.

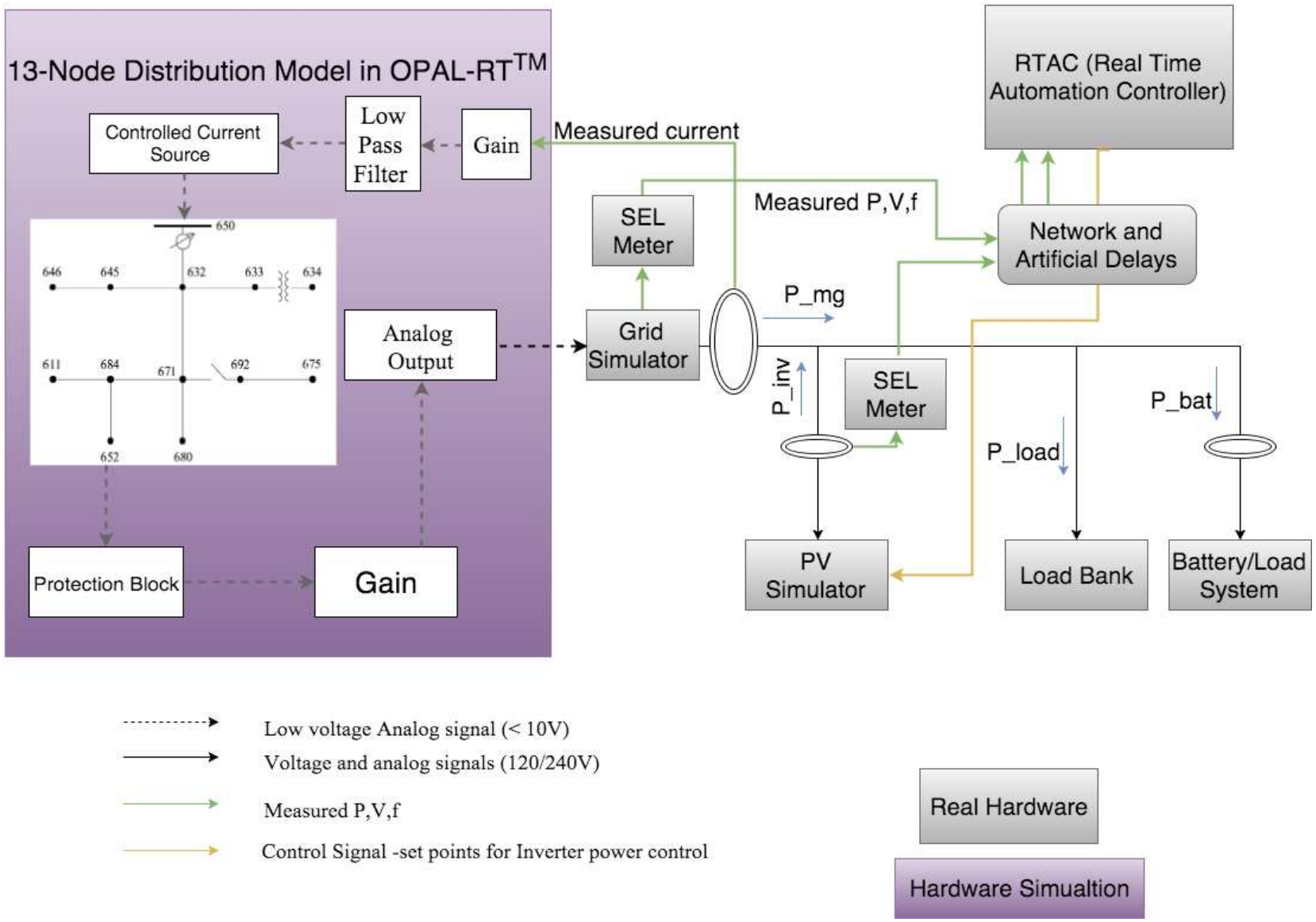

Figure 3.8: Power Hardware in the Loop setup and feedback from the Hardware.

Chapter 4

DISTRIBUTED ENERGY RESOURCES

4.1 INTRODUCTION

One of the aim of microgrid is combining all the benefits of the renewable generation technologies with the combined heat and power systems. Many countries are coming up with plans to reduce the carbon emissions to meet the global carbon emission commitment. Non-conventional generation system employed in the dispersed or distributed generation systems are known as DER or microsources. Choice of DER commonly depends on the availability of the fuel and topology of the region. This chapter describes the modeling process of the two DERs: (i) Diesel generator, and (ii) Solar Photovoltaic array. Though storage devices are not typical DERs, but for maximum benefit from the microgrid the application of storage device is mandatory with demand side management. For this reason a battery inverter system is also modeled which will be the energy storage device in the microgrid.

4.2 PHOTOVOLTAIC (PV) ARRAY PLANT

Solar PV generates electricity from inexhaustible solar energy. Some of the major advantages of PV system, includes (i) minimum environmental impact (ii) long functional life of over 30 years and (iii) reliable and sustainable nature of fuel. A PV plant is the combination of a PV inverter and PV arrays. MPPT (Maximum Power Point Tracking) which sets the voltage at such a point so that maximum power can be extracted form the PV array is used in the model. The standard Simulink^{TM} average inverter model was used in this simulation with a MPPT algorithm. A single

diode PV cell model was developed for real-time simulation, with the capability to vary output depending on ambient temperature, irradiance, and number of cell in series and parallel.

The PV array model available in Simulink™ has algebraic loops that the Simulink™ easily solves. However, these models were incompatible for real-time simulation in OPAL-RT™. This is because the C code necessary for executing models in OPAL-RT™ cannot be created for any model having an algebraic loop. Using a zero-order hold or a memory block can eliminate algebraic loops. A PV cell model was developed with the parameters from SunPower™ SPR-305-WHT available under the Simulink™ model library. Table 4.1 presents the parameters which are coded into MATLAB™ script for the PV cell, these parameters can be changed easily by changing the parameters in the script. The Matlab script is used by the RT-LAB™ model for the real-time simulation of the PV cell model.

Table 4.1: SunPower SPR™-305-WHT Parameters

SunPower™ SPR-305-WHT	
Parameter	Value
No. of series modules in string	5
No. of parallel modules in string	66
Voc	64.2
Isc	5.96
Vmp	54.7
Imp	5.58
Rs	0.037998
Rp	993.51
Isat	1.1753e-8
Iph	5.9602
Qd	1.3

A single diode model is developed based on (4.1) and (4.2). The circuit diagram for a single diode PV cell is shown in Figure 4.1, where I_0 is the saturation current, I_{pv} is the current generated directly proportional to solar irradiance, V_t is the thermal voltage of the array with N_s and N_p cells connected in series and parallel, q is the electron charge, k is the Boltzmann constant, T (in Kelvin)

is the temperature of the pn junction, and a is the ideality constant.

$$I = I_{pv} - I_0 \left[exp\left(\frac{V + I.R_s}{aV_t} \right) \right] - \frac{V + I.R_s}{R_p} \tag{4.1}$$

$$V_t = \frac{N_s KT}{q} \tag{4.2}$$

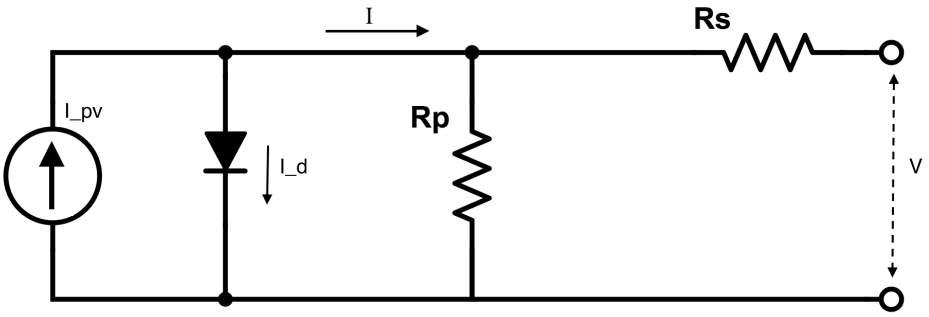

Figure 4.1: Single diode PV cell diagram.

The array temperature assumed constant at 30°C and the solar irradiance varies from 200-1000 W/m2, in steps of 100 W/m2, to obtain the I-V characteristics of the PV array model as shown in Figure 4.2. These I-V characteristics are compared with those of the original Simulink™ model [45] to verify the developed model and the relative percentage error is found to be 0.01% at the maximum power point, which was deemed acceptable for further use.

The models for the maximum power point tracking (MPPT) control, the boost converter, and the inverter were obtained from the Simulink™ demonstration example developed by MathWorks [45]. The MPPT control algorithm was based on the perturb-and-observe (P-O) technique from [46].

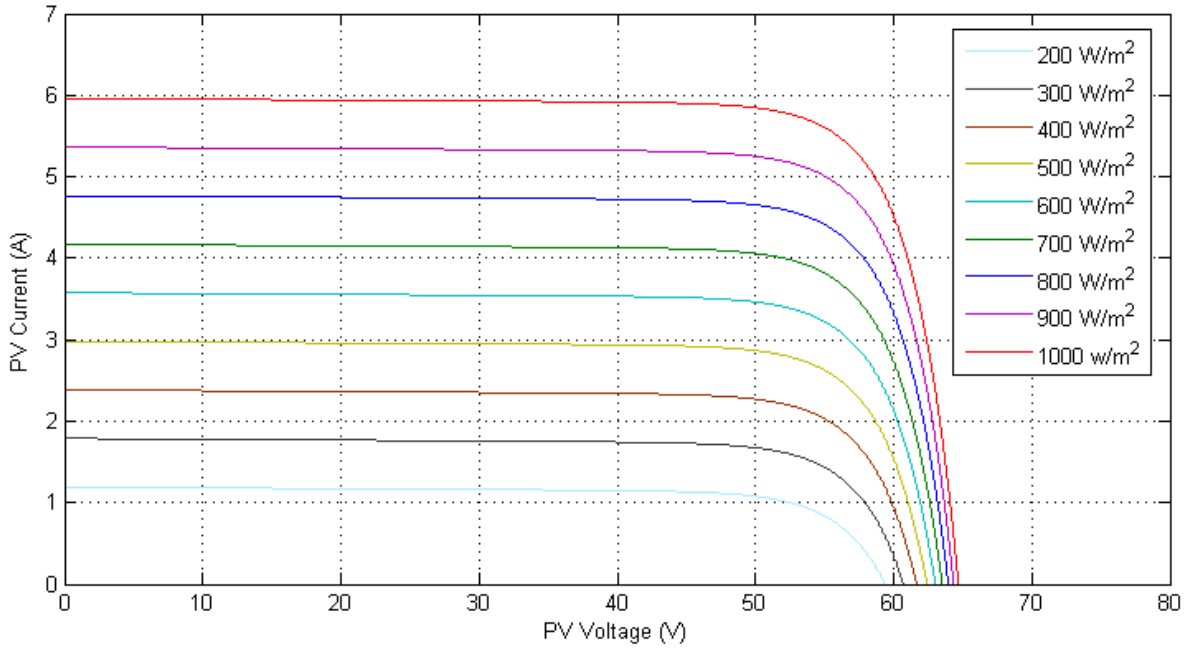

Figure 4.2: I-V curve for varying irradiance at 30°C.

VOLTAGE SOURCE CONVERTER (VSC) CONTROL

The conventional d-q control strategy is the most popular methodology, also known as dq current control [47]. The classical control is based on nested loop dq control scheme, which includes a dc voltage control and an inner current loop. The measured voltage and current are transformed into dq quantities and the outer control loop generates the dq current references [47]. The inner current loop regulates the dq current and generates the appropriate switching pulses. This control is implemented in VSC controller in the Simulink™ example model, which sends the reference waveforms to the average VSC model. Figure 4.3 shows the above discussed technique for VSC control.

An average VSC model was used for the simulation and this model does not require PWM switching, instead it used the reference voltage waveforms. The average VSC model is available under the Simpowesystem™ library. An average model of the inverter, where the inverter is modeled as current and voltage sources, was used for the simulation. The power and voltage levels

in the VSC controller of the inverter and the transformer coupling the PV array to the grid were changed according to the voltage level (4.16 kV) of the IEEE 13-Node distribution system.

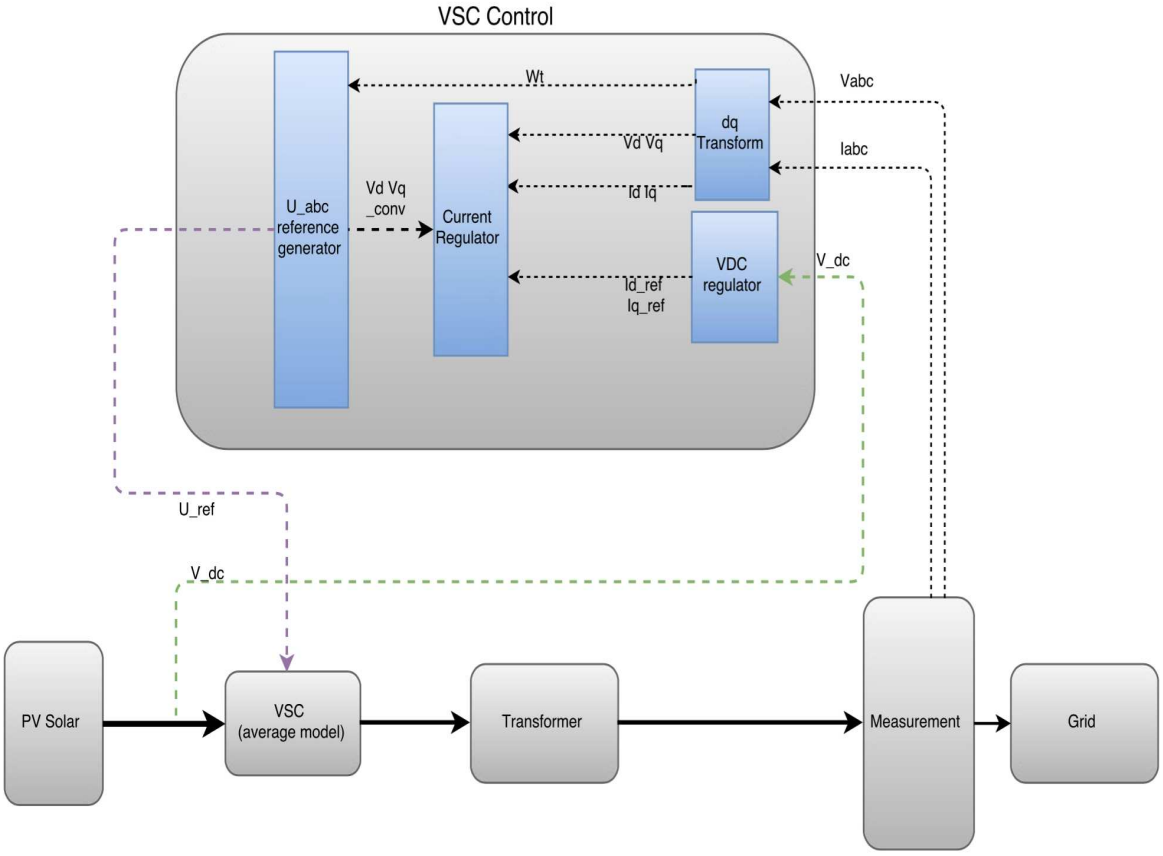

Figure 4.3: VSC control.

Validation: The inverter model with SunPower^{TM} SPR-305-WHT characteristics delivers 100 kW at 1000 W/m2 sun irradiance. The PV array was simulated with a varying irradiance in OPAL-RT^{TM}. A grid connected PV model consisting of two SunPower^{TM} SPR-305-WHT PV panel, delivering 200 kW, is simulated in OPAL-RT^{TM}. Figure 4.4 shows the varying irradiance profile and the output of the PV inverter, where we observe that as the irradiance increases, the output power from PV inverter also increases, in steps.

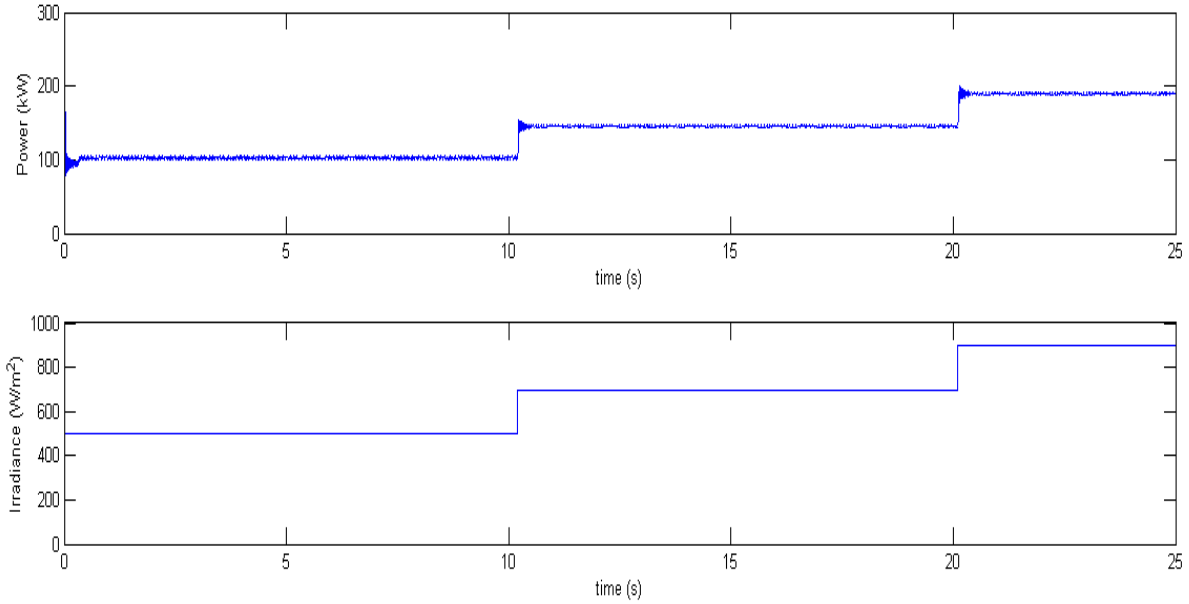

Figure 4.4: Variation of PV inverter output in grid connected mode with varying irradiance.

4.3 DIESEL GENERATOR

The synchronous generator model, available in the SimPowerSystems toolbox library of Simulink™, implements a 3-phase synchronous machine modeled in the dq reference frame [48]. This model takes the pu reference speed and the pu voltage reference as inputs. The governor and the exciter or the automatic voltage regulator (AVR) is responsible for controlling the current to the rotor field windings, which directly affects the terminal voltage of the generator [49].

The IEEE type 1 synchronous voltage regulator combined with an exciter is the excitation system implemented in this model. This model is developed by MathWorks which is based on [49]. One of the important changes to the model is the addition of a parasitic resistive load connected to the machine terminals to avoid numerical oscillations. This load is proportional to the time step of the simulation and the rating of the generator; for larger time steps, the parasitic load is bigger. The parasitic load is 2.5% of the nominal power rating for a 25 μs simulation time step of a 60 Hz system. In our case, for a 50 μs time step of a 60 Hz system with 3 MVA nominal

power, the parasitic load is 150 kW. Islanding a part of 13-Node distribution model with 3.577 MW load required a 3 MVA diesel generator. Synchronization of the diesel generator to the grid is done by matching the voltage, phase, and frequency. The phase sequence is assumed known. The Simulink^{TM} logical block and PLL blocks are used to measure the frequency and the phase of the oncoming generator and the grid. The synchronization parameters suggested by the IEEE 1547 std. are used [50], [1]. The synchronization switch/breaker is closed when the difference in frequency, f Hz, voltage, V %, and phase ϕ°, are less than 0.1 Hz, 3 %, and 10°, respectively. The control logic for synchronizing diesel generator to the grid is shown in Figure 4.5. The synchronization was performed with 13-Node distribution model with recording the frequency and the power of the system. It is observed that the phases lock into synchronism once the breaker is closed. The voltage output from generator is set at 1 pu and the frequency is set at 1.0001 for synchronization.The synchronization is smooth as seen from Figure 4.6, the voltage and current waveforms are smooth as expected.

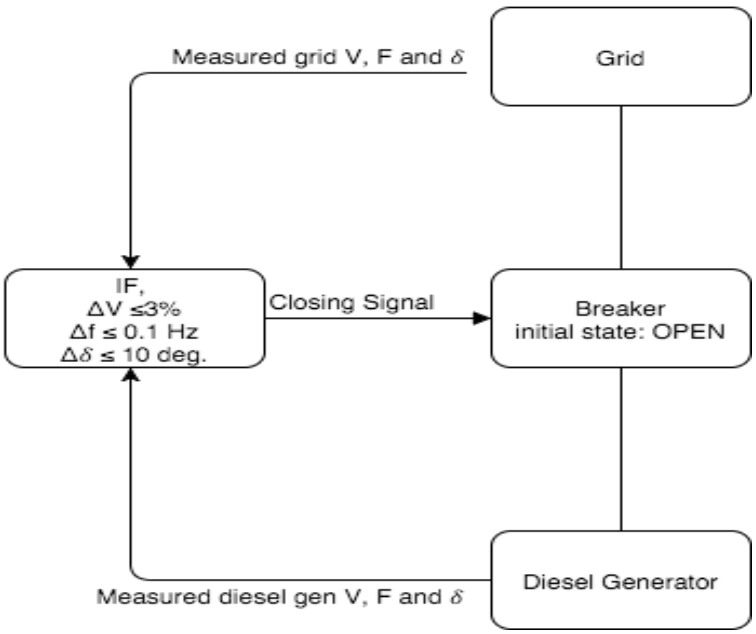

Figure 4.5: Synchronization control for diesel generator.

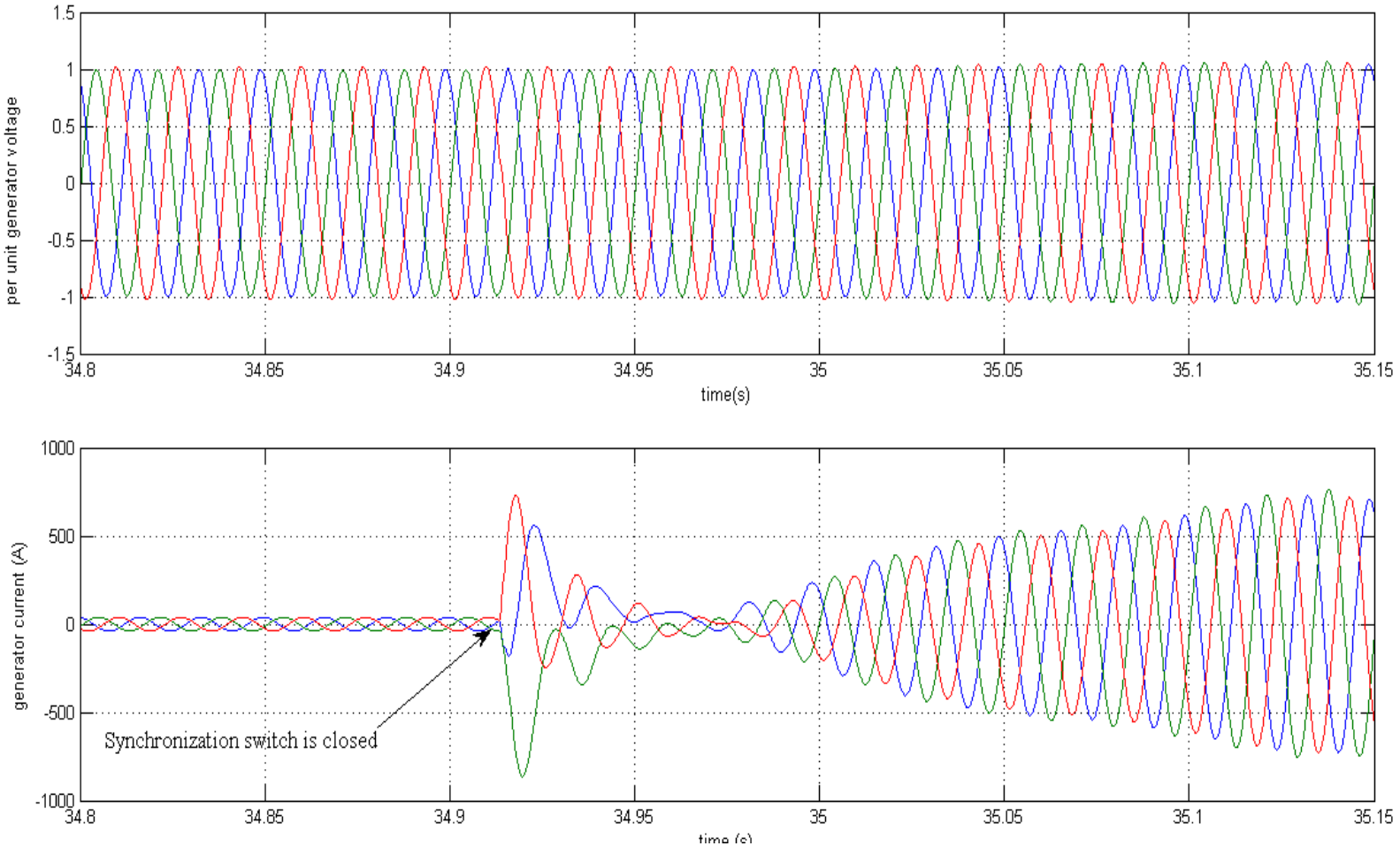

Figure 4.6: Voltage and current during diesel generator synchronization with 13-Node distribution model.

4.4 ENERGY STORAGE: BATTERY INVERTER SYSTEM

The energy storage system model comprises of a battery model and the inverter model. The standard battery model available under the Simulink^{TM} library [52] was used. Some of the changes to the battery model includes (i) Nominal battery voltage (V), (ii) State of charge (SOC) in percentage, (iii) Battery type, and (iv) Rated capacity of the Battery in ampere-hour (Ah).

Lead acid batteries are relatively economic but are prone to frequent maintenance and require relatively larger storage space. The life of these batteries tend to decrease if discharged below 30%. They are commonly installed in renewable and distributed power systems. The largest lead acid battery system installed is a 40 MWh system in California. The inverter model is similar to the inverter model in the PV array setup, however with some changes implemented for charging the battery. The battery inverter operates in the constant power mode, i.e., charging and discharging occur at a constant power specified in the VSC control block. The charging mode of the inverter is triggered by reversing the reference direct current (Id_ref) in the current regulator block of the VSC control block. This is shown in Figure 4.7.

The battery model is available under the Simulink^{TM} library is configured as lead-acid type battery at 500 V DC nominal voltage with 1000 Ah rated capacity. The internal resistance of the battery is calculated automatically by the Simulink^{TM} battery block based on the number of parallel and series combinations of the individual cell model, which is based on the nominal voltage and capacity of the battery model.

This battery model does not include self-discharge characteristics; hence, the discharge and charge characteristics of the battery are assumed same. The battery inverter system is connected to the IEEE 13-Node distribution system and operated in the charging and discharging mode in OPAL-RT^{TM} as shown in Figure 4.8. As expected the battery discharges and charges at a constant power of 500 kW with the state of charge (SOC) of the battery changing as expected for charging and discharging periods.

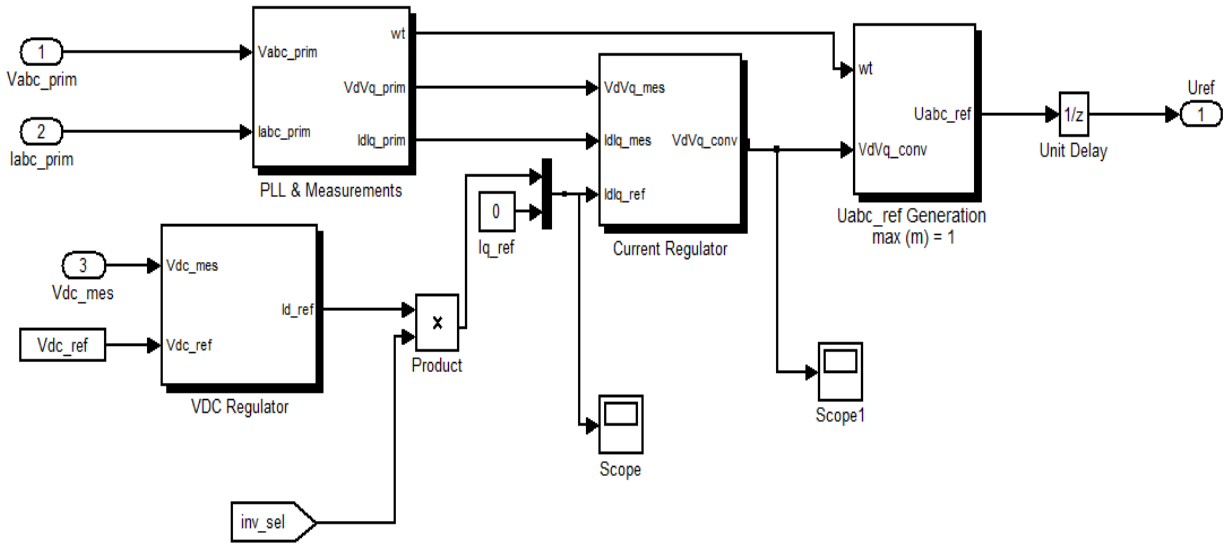

Figure 4.7: VSC control for battery charging and discharging.

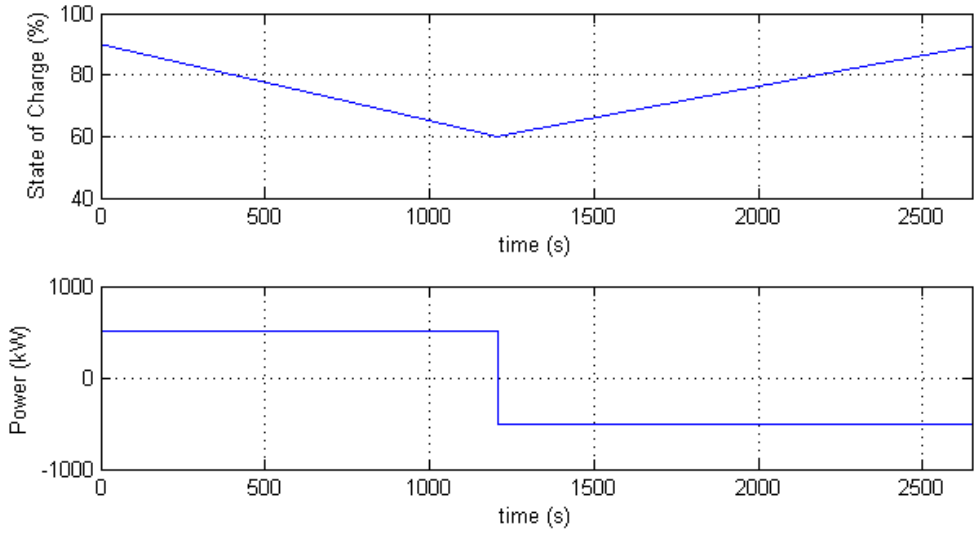

Figure 4.8: Change of Battery SOC with charging and discharging.

Chapter 5

MICROGRID

5.1 INTRODUCTION

U.S Department of Energy defines microgrid as: "A group of interconnected loads and distributed energy resources (DER) with clearly defined electrical boundaries that acts as a single controllable entity with respect to the grid (and can) connect and disconnect from the grid to enable it to operate in both grid-connected or island mode."

In transitioning microgrid to an islanded mode, it has to include a form of on-site power generation and/or energy storage. Without either, or both, a microgrid could not function properly. The distributed generation (DG) and energy storage become the foundation for the localized islanded microgrid. One of the other important components is the microgrid controller. Some of the important advantages of microgrids include:

1. Supporting the existing grid infrastructure by adding resilience to the grid infrastructure, compensating for local variable renewable sources, and supplying ancillary services such as reactive support and voltage regulation to a part of an Electric Power System (EPS).

2. Meeting uninterruptible power supply needs for critical loads, maintaining power quality and reliability at the local level, and promoting demand-side management.

3. Enabling grid modernization and interoperability of multiple smart-grid interconnections and technologies.

4. Integration of distributed and renewable energy resources to reduce carbon emissions, peak

load congestion, and line losses by locating generation near demand.

Microgrids are small-scale, low-voltage supply network for supplying heat and electrical loads to a small region. The generation technologies employed in a microgrid are usually renewable/ non-conventional resources integrated together to generate power at distribution voltages. These resources must be equipped with power electronic interfaces and control to ensure the operation of these resource as single aggregated system. This would allow the control of microgrid as single unit that meets the operation standards of the local utility. Microgrid is suitable for supplying power to the remote regions where supply from the grid is either difficult to avail or is not reliable due to severe weather conditions. Grid treats microgrid as a single controllable entity which can be operated as single aggregated load. This is important in ensuring reliability, security, and compliance with the local utility standards. However, to achieve a stable and secure microgrid operation, a number of technical and economic issues needs to be studied and researched.

Some of the common attributes of a microgrid are [51]:

1. It is not centrally planned and dispatched
2. It is usually smaller than 50MW
3. Power is directly fed to the utility
4. DERs are close to the consumers

The Simulink™ model of the DERs developed in this chapter forms a microgrid when connected to the 13-Node distribution model. All the above attributes of a microgrid are confirmed in the new microgrid. The diesel generator, the PV inverter system, and the battery storage system were connected to the 13-Node distribution system at nodes shown in Figure 5.1. The developed microgrid model was simulated in real-time on OPAL-RT™. The diesel generator was synchronized to the 13-Node distribution system with PV and battery inverter connected to the distribution system. The microgrid was islanded from the rest of the 13-Node distribution system with the

microgrid switch present between the nodes 632-671. Figure 5.2 shows power, frequency, and pu voltage at the instant of diesel generator synchronization to the 13-Node distribution system.

After synchronizing diesel generator to the 13-Node distribution system the microgrid is islanded. The active power from diesel generator raises to supply the microgrid power when microgrid is islanded. Figure 5.3 shows the pu voltage, frequency and power at the instant of islanding the microgrid and Figure 5.4 shows the values when the microgrid reaches a steady state values.

The islanded microgrid has voltage unbalance, requiring a voltage control strategy. One of the methods is to use capacitor banks to boost the voltage in the islanded microgrid because capacitor bank is the most economical solution for this type of problem. A microgrid controller model can control the switching of the Diesel generator, the PV and the battery. The microgrid controller should also control the switching of the capacitor bank when the microgrid is islanded for voltage control.

Microgrid requires a control to maintain system security and seamless transfer from one mode of operation to the other mode while maintaining the system and regulatory constraints. This is done via the use of microgrid controller. There can be a central controller and a microsources controller. The central controller controls the whole microgrid operation and the microsource controller controls the local DER operation. The power dispatch set points are set by the central controller for import and export of power based on some agreed contracts and economies.

A simple microgrid controller is developed which has has two basic functions (i) Protection and Co-ordination and (ii) Energy management. The energy management module provides the set point for the active power to the battery module according to the operational need of the microgrid. It is assumed that all power generated form the PV plant is utilized in the microgrid and the battery is managed to compensate for the change in load and PV plant output. The Protection and co-ordination is designed for an under voltage and an over voltage protection mechanism.

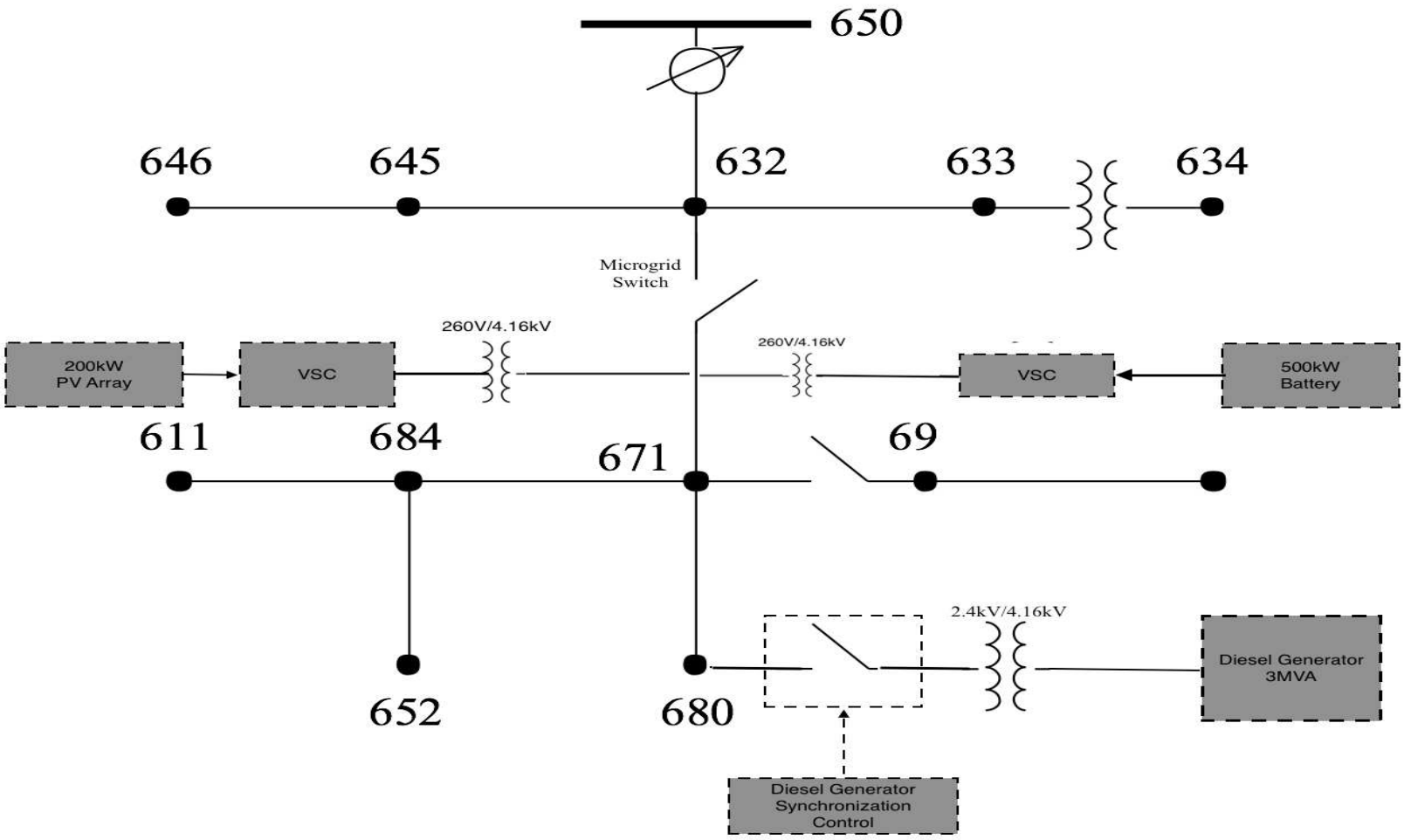

Figure 5.1: Microgrid with DERs and microgrid switch connected to 13-Node distribution model.

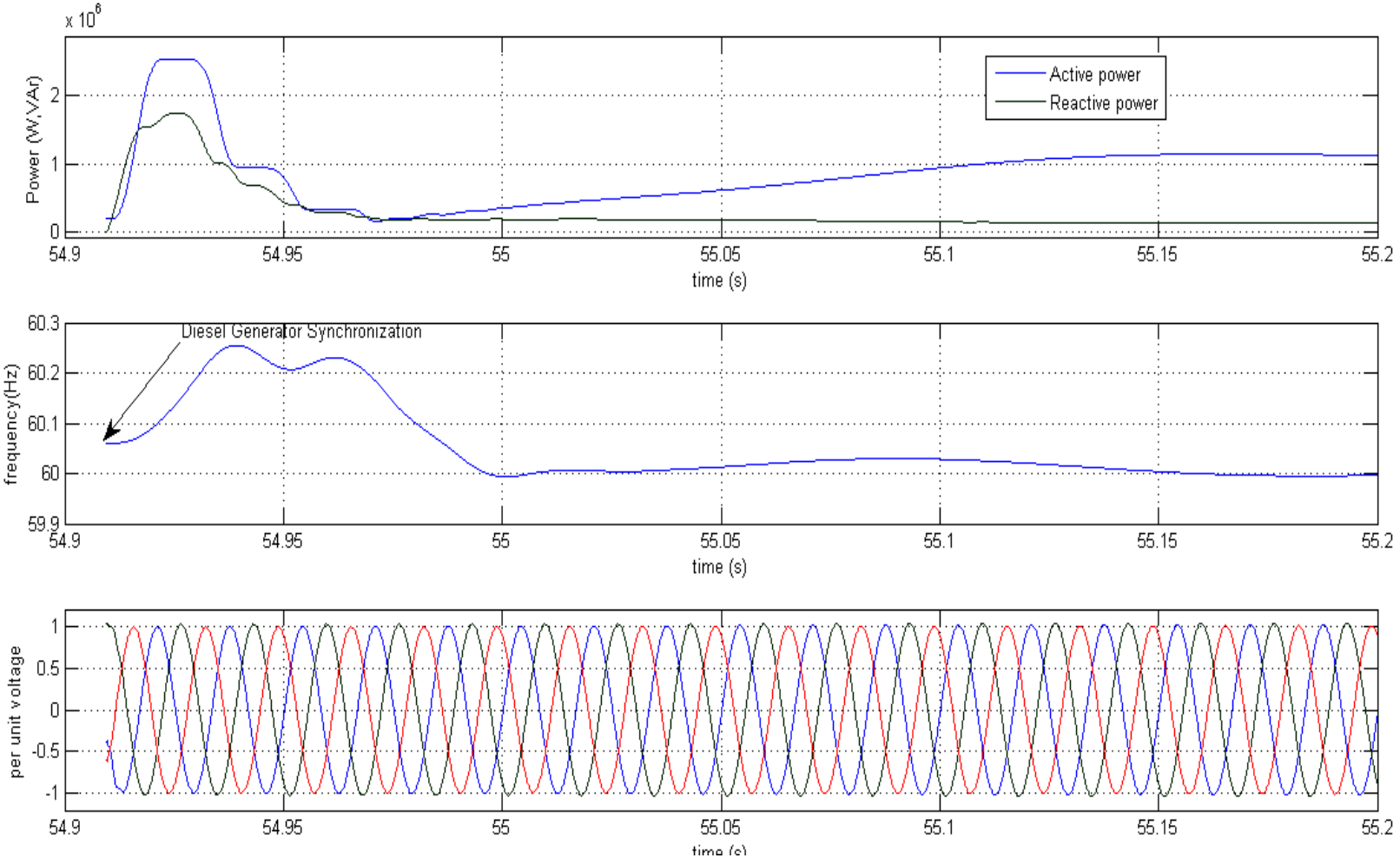

Figure 5.2: Diesel generator synchronization to 13-Node distribution.

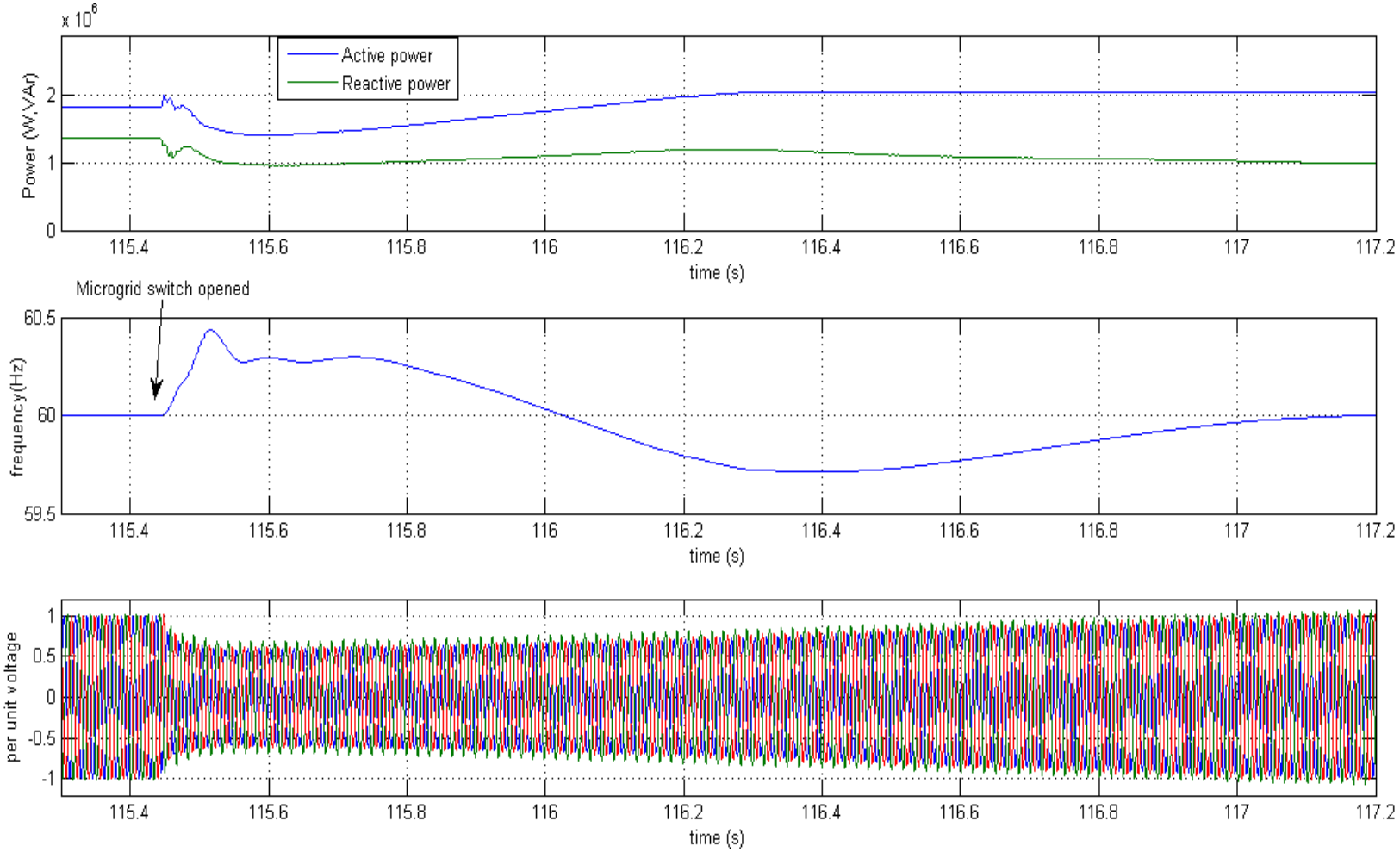

Figure 5.3: Power, pu voltage, and frequency variation when microgrid is islanded.

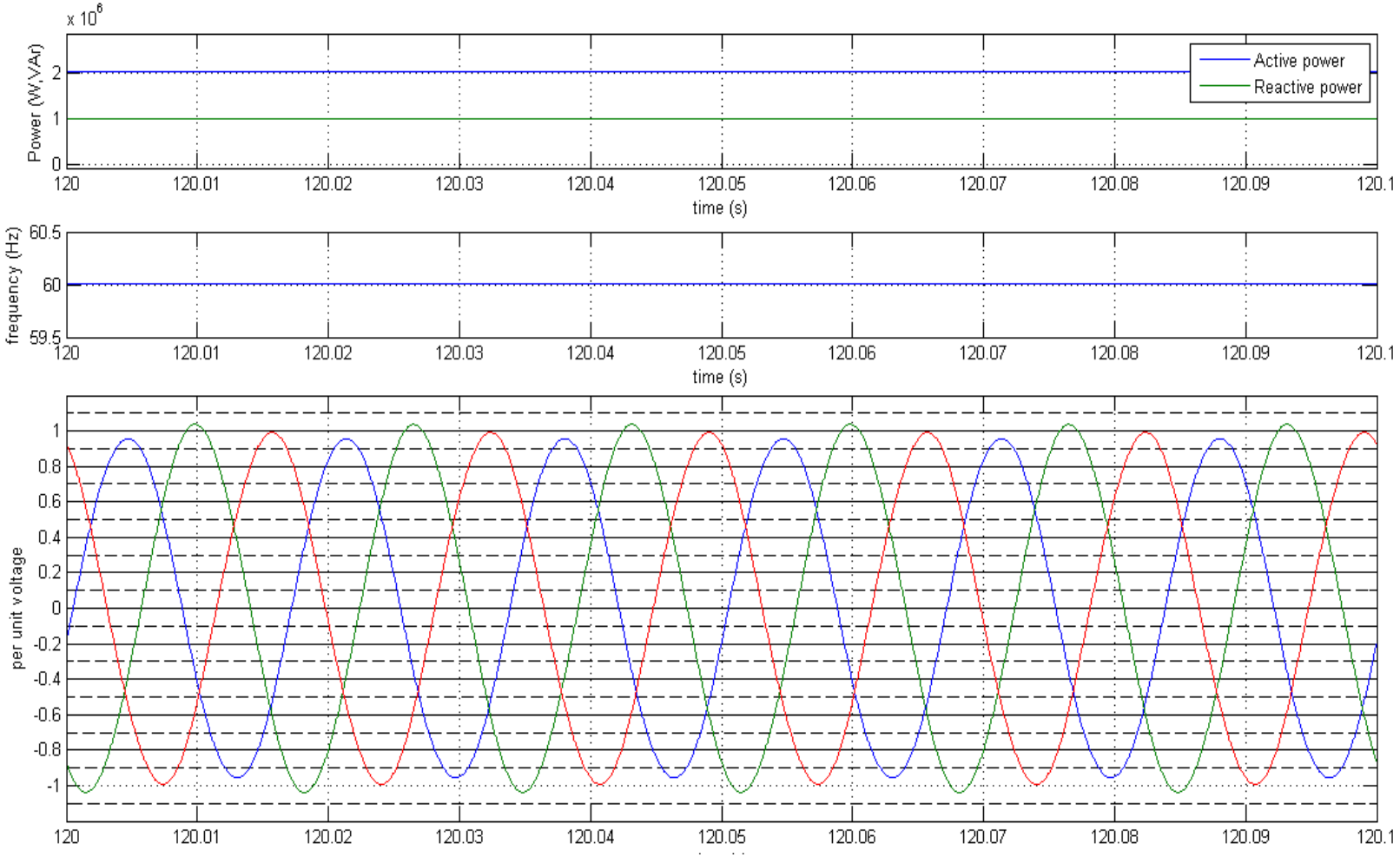

Figure 5.4: Power, pu voltage, and frequency when microgrid reaches a steady state.

The IEEE STD 1547.4-2011 has discussion on microgrid synchronization. The recommended voltage limits for resynchronization should be with in the "Range B of the ANSI/NEMA C84.1-2006, Table-1" and frequency range should be between 59.3 Hz and 60.5 Hz. The voltage, frequency and should be with in acceptable limits specified in the IEEE STD 1547-2003. There should be a 5 minute delay between the reconnection after the steady state voltages and frequency are achieved.

According to [53], which used the IEEE STD 1547-2003 as the basis of its interconnection guidelines, the steady operating range for the distribution system above 1 kV is $\pm 6\%$ and nominal system frequency range between ± 0.2 Hz. The voltage unbalance should be below 3% under normal operating conditions. Equation (5.1) gives the voltage unbalance equation.

$$\text{Voltage unbalance } (\%) = \frac{\Delta V_{max}}{V_{avg}} \tag{5.1}$$

where V_{avg} is the average of the three phases and ΔV_{max} is the maximum deviation from average phase voltage. The pu voltages of all the nodes in the microgrid are shown in Table 5.1. The maximum % voltage unbalance calculated at all the three phase nodes is 6.3% which is outside the range of the 3% deviation, which is not acceptable. It can be observed form Table 5.1 that voltage needs to raised to satisfy the unbalance requirement of less than 3% and also to raise the voltages to facilitate resynchronization of microgrid to the grid. The voltages before capacitor bank switching are not in the range of $\pm 3\%$. Table 5.1 gives the values of the voltages after capacitor bank switching. After the switching of capacitor bank the maximum voltage unbalance is 1.6% on the phase A of node-680. The unbalance in the microgrid is well with the unbalance range of 4% and steady state pu voltages are with in the the range of $\pm 6\%$ after the capacitor bank is switched in the microgrid, a time delay of 1s is introduced before the capacitor bank switching to minimize any transients. The voltages are found to be in acceptable range according to the standards discusses above.

Table 5.1: Microgrid pu voltages

Node	Phase	pu voltage with Capacitor bank	pu voltage with Capacitor bank
Node-680	A	1.045827	1.009347
Node-680	B	0.970457	0.980505
Node-680	C	0.938214	0.990986
Node-684	A	0.960788	0.983091
Node-684	C	0.958724	0.982374
Node-611	C	0.932919	0.980369
Node-652	A	0.939920	0.97753
Node-692	A	1.040354	0.984943
Node-692	B	0.962769	0.981651
Node-692	C	0.932788	0.984338
Node-675	A	1.042625	0.978429
Node-675	B	0.960861	0.98383
Node-675	C	0.982394	0.982394

5.2 ANALYSIS OF PASSIVE SYNCHRONIZATION

Passive synchronization requires sensing of voltage, frequency, and phase angle on both the microgrid and the grid side. Synchrocheck relay is used for this purpose which measures the difference in voltage, frequency, and phase angle on both sides. Passive synchronization methods may take longer than the active synchronization, where a control mechanism matches the voltage, frequency, and the phase angle of the microgrid to the grid. In order to guarantee the synchronization and possible reconnection a small frequency error 0.001 pu is intentionally introduced through the diesel generator speed set points. Figure 5.5 and Figure 5.6 shows resynchronization of the microgrid to the grid. The maximum frequency and the voltage deviation is well within the limit. Also, there is no overshoot in the power as there is less than 20% of the power imported from the grid. In case there is an overshoot in the power, the DER might reach its power limit and cause tripping of the equipment.

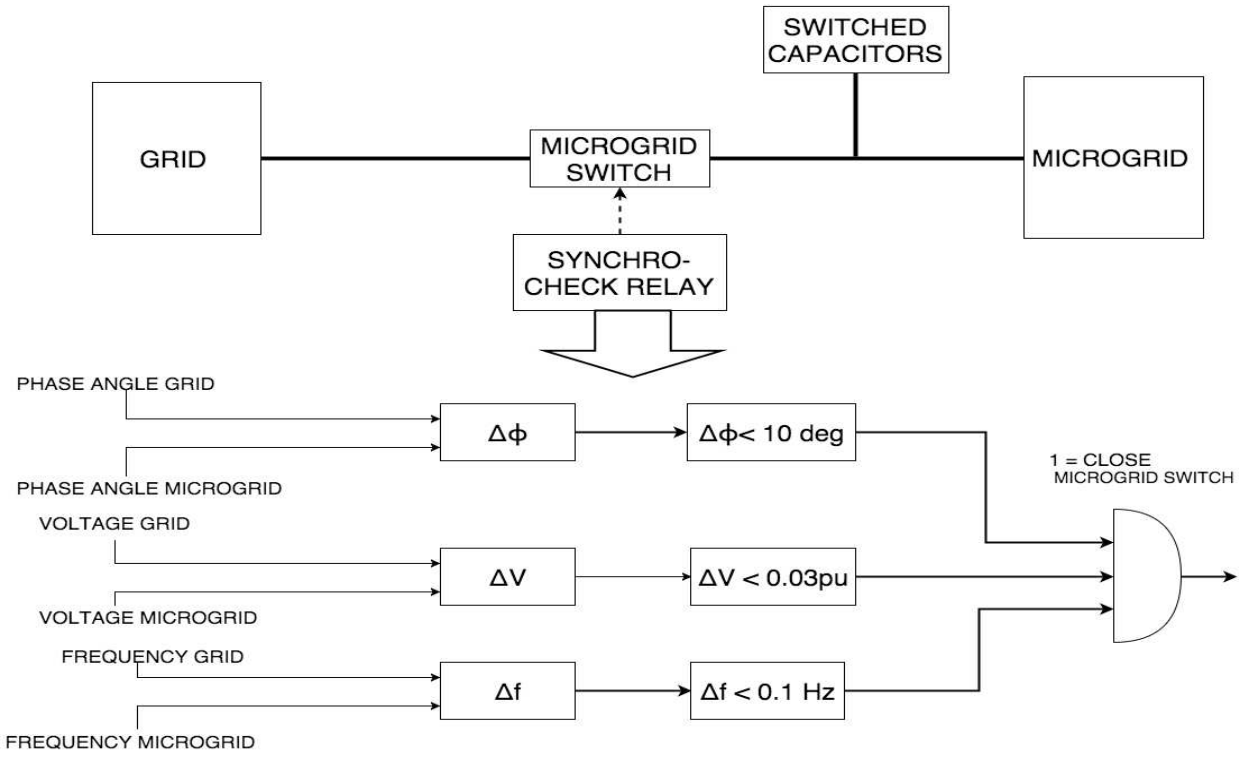

Figure 5.5: Synchronization mechanism for the microgrid.

5.3 PROTECTION

Reference [53] utilizes IEEE 1547 as the basis for interconnection and mentions that the under-voltage/over-voltage protection must have the ability to detect phase to ground voltage that is outside the normal operating limits of 90% $<$ V $<$ 106% of the nominal and must trip within the trip time mentioned in the Table 5.2. Two scenarios for under-voltage were simulated, in the first case there is a 3-phase line to ground fault with 0.001 Ω fault resistance at the node-632. This causes the voltage to drop below 50% of the nominal. This causes the the trip signal to the breaker and the microgrid is islanded. Figure 5.7 shows the voltage and frequency of the microgrid and the grid before.

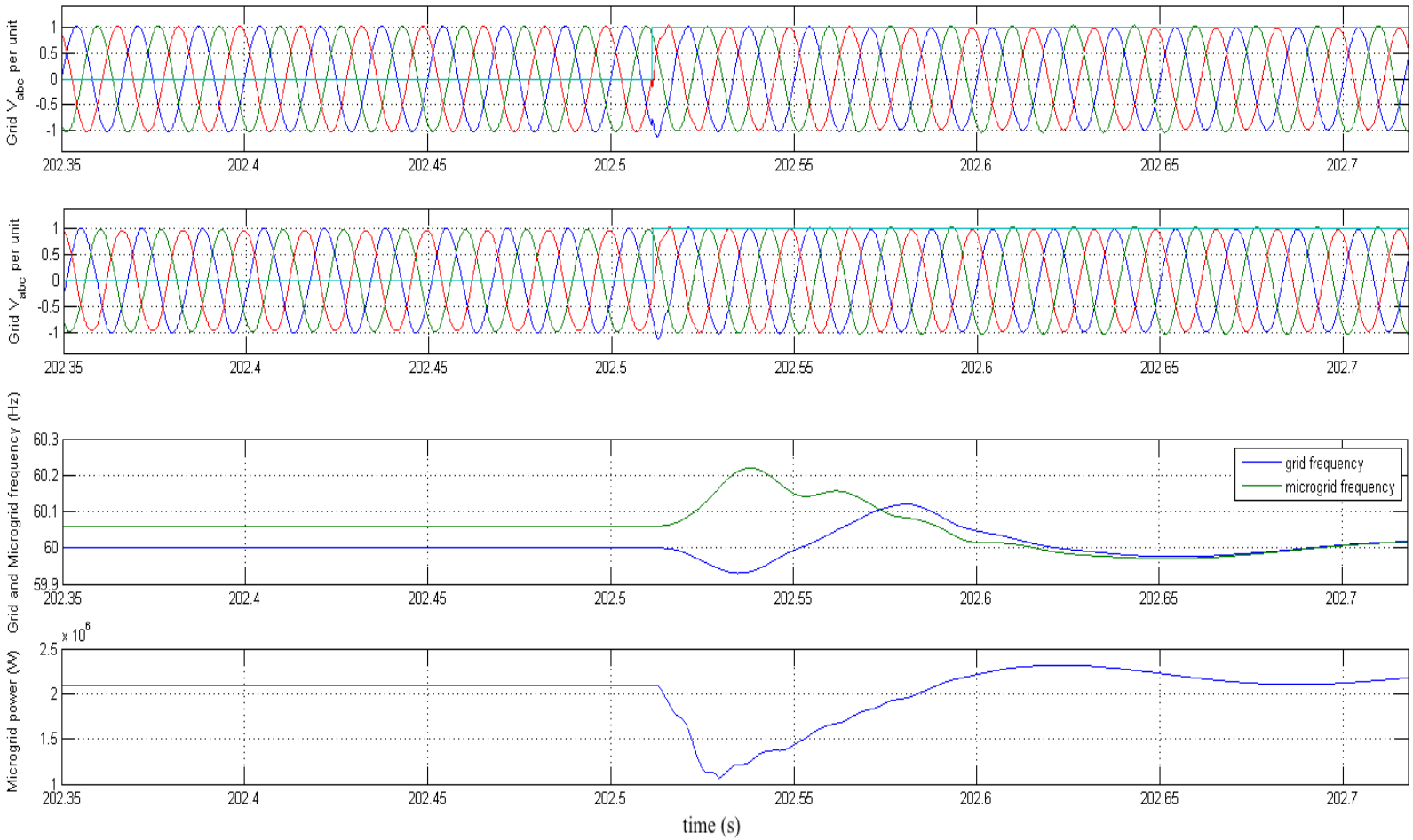

Figure 5.6: pu voltages and frequency during synchronization of microgrid to the grid.

In the second case there is a 3 phase line to ground fault on the node-632 with 0.4 Ω fault resistance. This cause the voltage to drop at 80% of the nominal voltage. There is no intentional delay introduced, but there is a delay between the tripping of the breaker and the fault because it takes at least one cycle to calculate the rms values of the signals. In figure 5.8, at time 640.075 s, the 3-phase line to ground fault occurs on the main grid then at 640.086 s Microgrid switch is opened, islanding the microgrid. At time 640.18 s, the microgrid voltages becomes stable. It can be observed that the steady voltages are with in the specified range of $\pm$ 6% and the frequency is with in 59.3 Hz and 60.5 Hz.

Table 5.2: under-voltage/over-voltage protection.

PU voltage	Trip time
V $\leq$ 50%	Instantaneous
50% $<$ V $<$ 90%	120 cycles
90% $<$ V $<$ 106%	Normal Operation
106% $<$ V $<$ 120%	30 cycles
V $\geq$ 120 %	Instantaneous

5.4 ENERGY MANAGEMENT

The battery power set points are set according to the PV and load variation in the microgrid. It is assumed that diesel generator set points are already set by the management agent. The load within microgrid may change at any time, in order to keep the power balance between load and generation, the controller should be able to handle any load change within its capability.

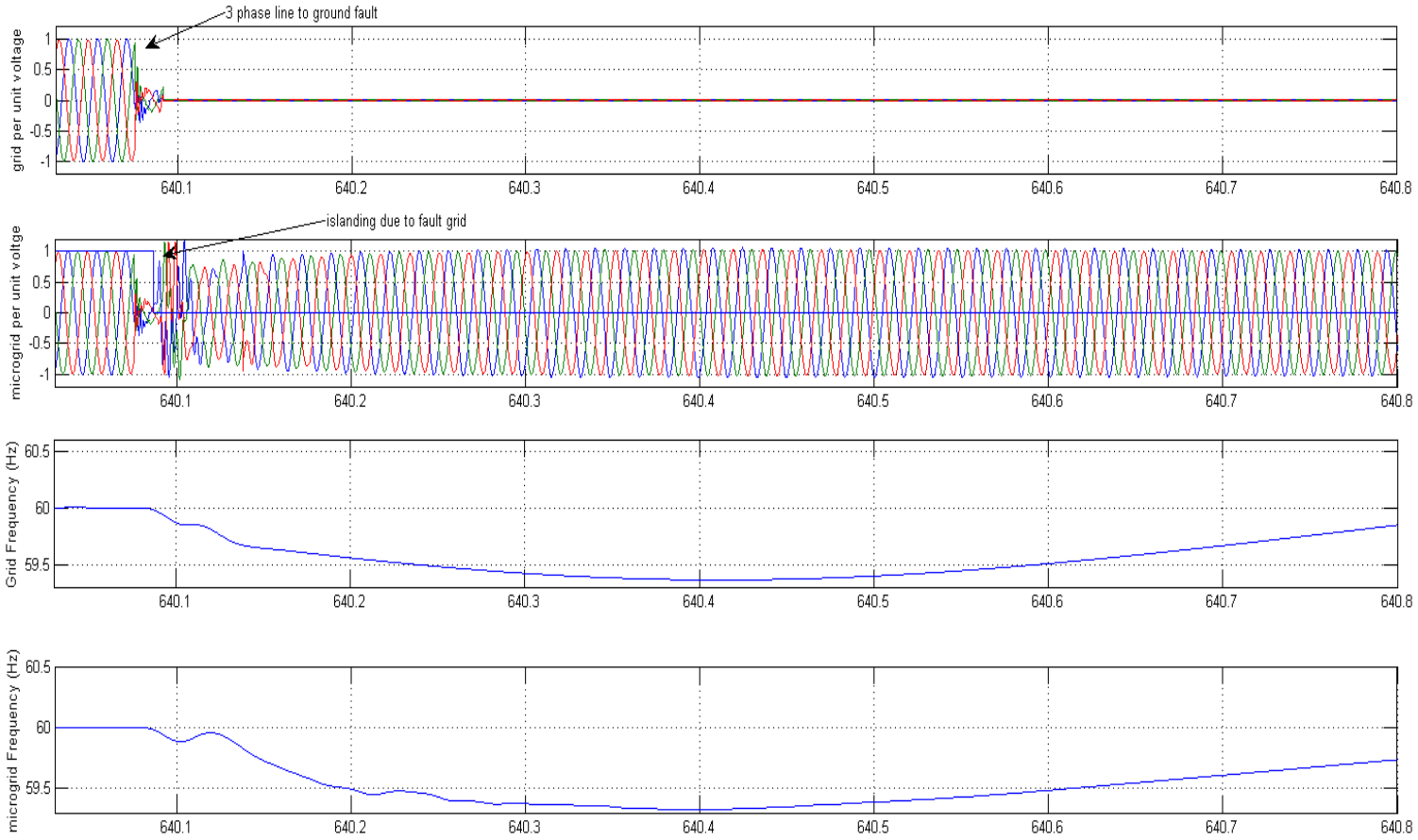

Figure 5.7: Pu voltage and frequency during 3-phase fault on the grid (V $<$ 50%).

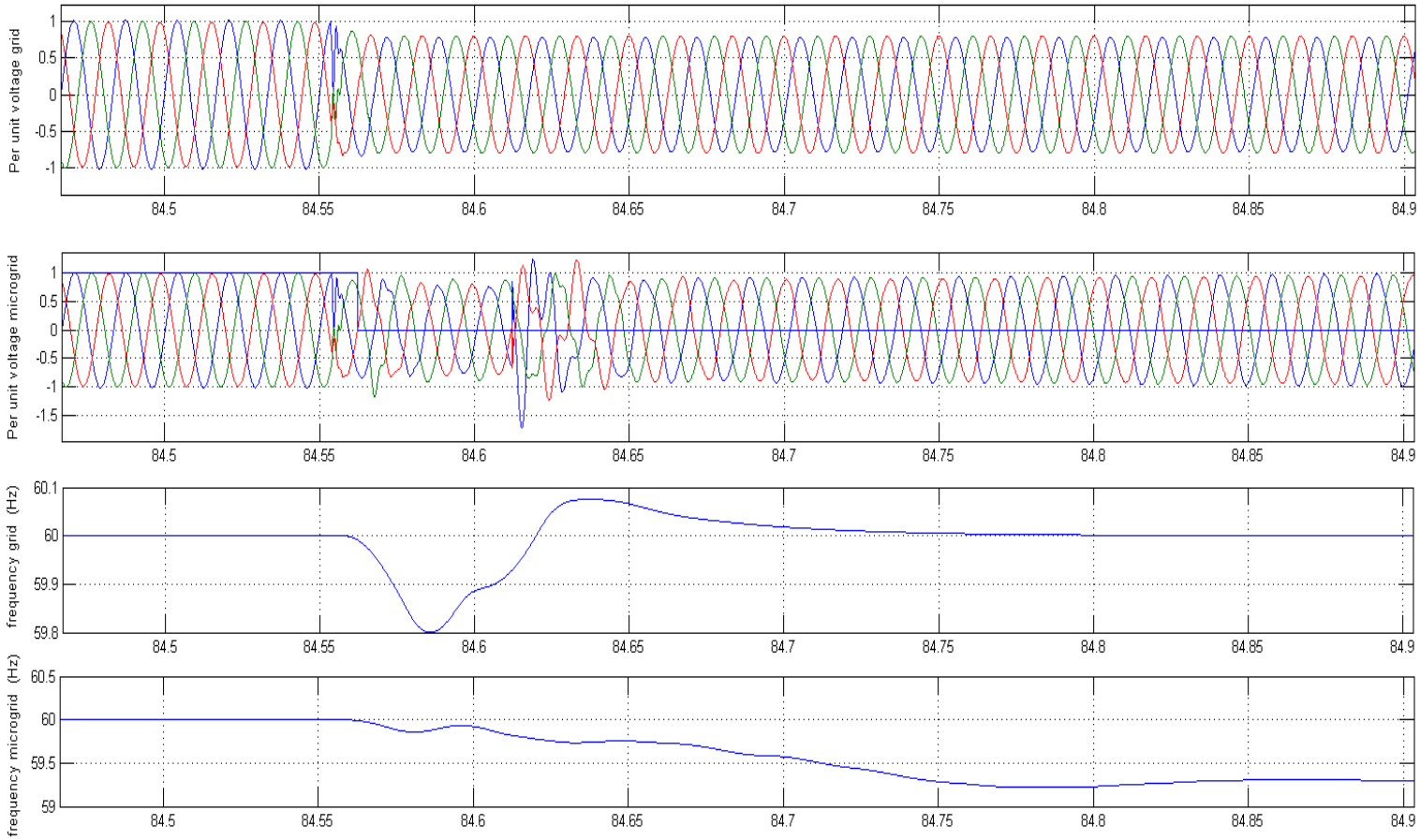

Figure 5.8: Pu voltage and frequency during 3-phase fault on the grid (V $<$ 80%).

It is expected that the battery should take the responsibility to maintain power balance within the microgrid. This includes the the variation in the power of the PV array from the nominal and any load variation. Figure 5.9 shows the variation of the load in the microgrid and the variation of the irradiance causing the change in the power output of the battery. It can be seen that battery can quickly track the variation in the load and performs as expected. The battery power output set points are set according to the equation (5.2).

$$P_{set}(kW) = \Delta P_{load} + \Delta PPV \tag{5.2}$$

where, P_{set} is the battery setpoint in kW, ΔP_{load} is the change in load in the microgrid, and ΔP_{PV} is the change in the PV output from the nominal values.

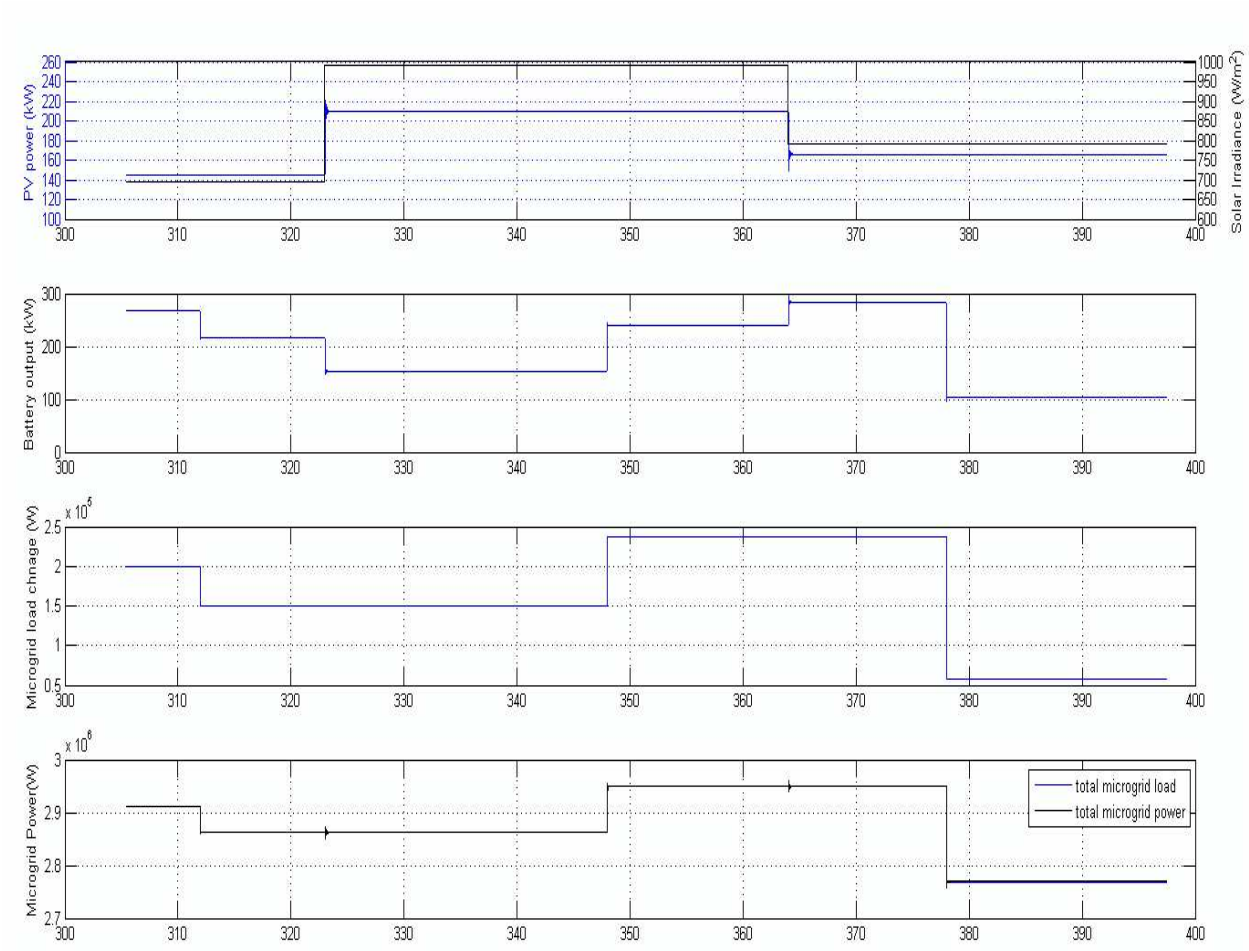

Figure 5.9: Power management by the microgrid controller with variation in microgrid load and PV array.

Chapter 6

Conclusion and Future Work

6.1 CONCLUSION

A real-time model of the IEEE 13-Node distribution feeder network was developed, simulated, and quantified on a real-time platform OPAL-RT™ using Simulink™ library. Multi-core simulation for 13-Node distribution model was performed and verified with relative absolute pu voltage error less than 2.5%. Modeling and simulation challenges of the real-time model were addressed. A diesel generator, a PV array model, and a battery inverter system models were developed and simulated on a real-time platform. The diesel generator synchronization control was developed and tested in OPAL-RT™. DERs were connected to the 13-Node distribution model forming a microgrid. A simple microgrid controller with two basic function of protection-coordination and energy management was developed. The microgrid was islanded from the 13-Node distribution system and the steady state state values of the microgrid were observed as expected from the calculations of load in the microgrid. Two common scenarios of intentional and unintentional islanding were successfully performed. Appendix-A.7 lists the Simulink™ and RT-LAB™ model developed and included with this report.

6.2 FUTURE WORK

The state space nodal (SSN) type OLTC developed by OPAL-RT™ can eliminate any overruns in the IEEE 13-Node distribution model and the distribution model will not require splitting of the model into two cores. A simple microgrid controller to control the DERs, islanding mode, and

grid-tied mode of microgrid will be the next step in modeling, which will complete the microgrid model. The DERs developed in the OPAL-RT^{TM} can be replaced with the actual hardware and the results of the power hardware-in-the-loop (PHIL) tests can be compared with the simulation results. Further, a variety of what-if scenarios may be studied in this test setup to aid in full characterization of such emerging microgrid systems. This model can then be used to implement dispatch algorithms for the microgrid to operate in grid-tied and islanded modes, and eventually performing HIL simulations.

References

[1] H. E. Brown, S. Suryanarayanan, G. T. Heydt, "Some characteristics of emerging distribution systems considering the Smart Grid Initiative," *The Electricity Journal*, v. 23, no. 5, June 2010, pp. 64-75.

[2] S. Suryanarayanan, F. Mancilla-David, J. Mitra, Y. Li, "Achieving the Smart Grid through customer-driven microgrids supported by energy storage," in *Proc. 2010 IEEE Int'l Conference on Industrial Technologies (ICIT)*, Viadel Mar, Chile, pp. 884-890.

[3] S. Suryanarayanan, M. Steurer, S. Woodruff, R. Meeker, "Research perspectives on high-fidelity modeling, simulation, and hardware-in-the-loop for electric grid infrastructure hardening," in *Proc. 2007 IEEE Power Engineering Society (PES) General Meeting*, 4 pp., Jul 2007.

[4] H. W. Dommel, "Digital Computer Solution of Electromagnetic Transients in Single-and Multiphase Networks," *IEEE Transactions on Power Apparatus and Systems*, vol. PAS-88, pp. 388-399, Apr. 1969.

[5] C. Dufour, S. Abourida, J. Blanger, "InfiniBand-Based Real- Time Simulation of HVDC, STATCOM and SVC Devices with Custom-Off-The-Shelf PCs and FPGAs," in *Proc. 2006 IEEE International Symposium on Industrial Electronics*, pp. 2025- 2029.

[6] Y. Liu, et al., "Controller hardware-in-the-loop validation for a 10 MVA ETO-based STATCOM for wind farm application," in *IEEE Energy Conversion Congress and Exposition (ECCE09)*, San-Jos, CA, USA, pp. 1398-1403.

[7] J.N. Paquin, J. Moyen, G. Dumur, V. Lapointe, "Real-Time and Off-Line Simulation of a Detailed Wind Farm Model Connected to a Multi-Bus Network", *IEEE Canada Electrical Power Conference 2007*, Montreal, Oct. 25-26, 2007.

[8] J.N. Paquin, C. Dufour, and J. Blanger, "A Hardware-In-the- Loop Simulation Platform for Prototyping and Testing of Wind Generator Controllers" in *2008 CIGRE Conference on Power Systems*, Winnipeg, Canada. October 19-21, 2008.

[9] V.K Sood, D, Fischer, J.M Eklund, T. Brown, "Developing a communication infrastructure for the Smart Grid," in *Electrical Power & Energy Conference (EPEC), 2009 IEEE*, pp.1-7, 22-23 Oct. 2009.

[10] Nikos Hatziargyriou, Hiroshii Asano, Reza Iravani, Chris Marnay, "Microgrids IEEE Power and Energy Magazine", 5 (4) (2007), pp. 78-94.

[11] H. Nikkhajoei, R. H. Lasseter Distributed generation interface to the CERTS microgrid IEEE Transaction on Power Delivery, 24 (3) (July 2009), pp. 1598-1608.

[12] S. Chakraborty, M. D. Weiss, and M. G. Simoes, "Distributed intelligent energy management system for a single-phase high-frequency AC microgrid," *IEEE Trans. Ind. Electron.*, vol. 54, no. 1, pp. 97-109, Feb. 2007.

[13] A. G. Tsikalakis and N. D. Hatziargyriou, "Centralized control for optimizing microgrids operation," *IEEE Trans. Energy Convers.*, vol. 23, no. 1, pp. 241-248, Mar. 2008.

[14] E. Barklund, N. Pogaku, M. Prodanovic, C. H. Aramburo, and T. C. Green, "Energy management in autonomous microgrid using stabilityconstrained droop control of inverters," *IEEE Trans. Power Electron.*, vol. 23, no. 5, pp. 2346-2352, Sep. 2008.

[15] J. Stevens, H. Vollkommer, D. Klapp, "CERTS microgrid system tests," in *Proc. IEEE Power Eng. Soc. Gen. Meet. 2007*, Jun., pp. 1-4.

[16] D. K. Nichols, J. Stevens, and R. H. Lasseter, "Validation of the CERTS microgrid concept the CEC/CERTS microgrid testbed," in *Proc. IEEE Power Eng. Soc. Gen. Meet. 2006*, Jun., pp. 18-22.

[17] N. Pogaku, M. Prodanovic, T. C. Green, "Modeling, analysis and testing of autonomous operation of an inverter-based microgrid," *IEEE Trans. Power Electron.*, vol. 22, no. 2, pp. 613-625, Mar. 2007.

[18] M. Meiqin et al., "Testbed for microgrid with multi-energy generators," in *Proc. Can. Conf. Electr. Comput. Eng*., May 2008, pp. 637-640.

[19] B. Kroposki, R. Lasseter, T. Ise, S. Morozumi, S. Papatlianassiou, and N. Hatziargyriou, "Making microgrids work," *IEEE Power Energy*, vol. 6, no. 3, pp. 40-53, May/Jun. 2008.

[20] J. Arai, K. Iba, T. Funabashi, Y. Nakanishi, K. Koyanagi, and R. Yokoyama, "Power electronics and its applications to renewable energy in Japan," *IEEE Circuits Syst.*, vol. 8, no. 3, pp. 52-66, Sep. 2008

[21] C. Marnay, G. Venkataramanan, M. Stadler, A. S. Siddiqui, R. Firestone, B. Chandran, "Optimal technology selection and operation of commercial-building microgrids," *IEEE Trans. Power Syst.*, vol. 23, no. 3, pp. 975-982, Aug. 2008.

[22] B. Lu, X. Wu, H. Figueroa, and A. Monti, "A low-cost real-time hardwarein-the-loop testing approach of power electronics controls," *IEEE Trans. Ind. Electron.*, vol. 54, no. 2, pp. 919-931, Apr. 2007.

[23] W. Lee, M. Yoon, and M. Sunwoo, "A cost- and time-effective hardware-in-the-loop simulation platform for automotive engine control systems," *J. Automobile Eng.*, vol. 217, no. 1, pp. 41-52, 2002.

[24] J. Du, Y. Wang, C. Yang, and H. Wang, "Hardware-in-the-loop simulation approach to testing controller of sequential turbocharging system" ,in *Proc. 2007 IEEE Int. Conf. Autom. Logistics*, Aug. 2007, pp. 2426-2431.

[25] A. Guzman, S. Samineni, and M. Bryson, "Protective relay synchrophasor measurements during fault conditions," in *Proc. Power Syst. Conf.: Adv. Metering, Prot., Control, Commun. Distrib. Resour.*, Clemson, SC, Mar. 2006, pp. 83-95

[26] T. Bi, Y. Zhang, X. Xiao, P. Forsyth, and R. Wierckx, "Large scale power system simulation and PMU testing using a real time digital simulator," presented at the *IPEC 2007*, Singapore, Dec.

[27] I. F. Abdulhadi, R. M. Tumilty, G. M. Burt, and J. R. McDonald, "A dynamic modeling environment for the evaluation of wide area protection systems," presented at the 43rd Int. Univ. Power Eng. Conf. (UPEC 2008), Padova, Italy, Sep.

[28] M. Yu and H. Konishi, "The real time digital simulation of a single phase voltage source converter and its application," presented at the IPST 2003, New Orleans, LA, Oct. Paper No. 13-2.

[29] T. K. Kim, Y. B. Yoon, J.-B. Choo, R. Kuffel, and R. Wierckx, "Development and testing of a large scale digital power system simulator at KEPCO," in Proc. IPST 2001, Rio de Janeiro, Brazil, Jun., pp. 704-709

[30] S. Boshoff, C. van Dyk, L. Becker, M. Halonen, S. Rudin, J. Lidholm, and Dr T. Maguire, "SVC for resonance control in NamPower electrical power system," in Proc. IEE/PES Summer Meet. 2001, Vancouver, Canada, Jul., vol. 1 pp. 860-865.

[31] Y. B. Yoon, T. K. Kim, S. T. Cha, R. Kuffel, R. Wierckx, and M. Yu, "HVDC control and protection testing using the RTDS simulator," in Proc. 4th Int. HVDC Transm. Oper. Conf., Yichang, China, Sep. 2001, Paper No. 17, pp. 101-106.

[32] K. Miu, M. Klienberg, "Impact studies of unbalanced multi-phase distribution system component models," in *Proc. 2010 IEEE Power & Energy Society (PES) General Meeting*, 4 pp., Jul 2010.

[33] T. H. Chen, M. S. Chen, K. J. Hwang, P. Kotas, E. A. Chebli, "Distribution system power flow analysis-a rigid approach," *IEEE Transactions on Power Delivery*, vol. 6, no. 3, Jul 1991.

[34] IEEE Distribution Planning Working Group Report, Radial distribution test feeders, *IEEE Transactioins on Power Systems*, August 1991, Volume 6, Number 3, pp 975-985.

[35] IEEE Power & Energy Society (PES). Distribution test feeders. [Online] {Available} http://ewh.ieee.org/soc/pes/dsacom/testfeeders/(Accessed: Sep 18, 2015).

[36] MathWorks.SimPowerSystem.[Online] {Available}http://www.mathworks.com/products/simpower/

[37] MathWorks. Three-Phase Dynamic Load. [online]{Available}: http://www.mathworks.com/help /physmod/sps/powersys/ref/ threephasedynamicload.html (Accessed: Sep 18, 2015).

[38] MathWorks. Single Phase Dynamic Load [online] {Available}: http://www.mathworks.com/help /physmod/sps/examples/single-phase-dynamic-load-block.html

[39] MathWorks. OLTC Regulating Transformer (Phasor Model). [online]{Available}:http://www.mathworks.com/help/physmod/sps/examples /oltc-regulating-transformer-phasor-model.html (Accessed: Sep 18, 2015).

[40] W. H. Kersting. Distribution System Modeling and Analysis, 2nd Ed., CRC Press, 2007.

[41] MathLab.Electrical Distribution System Modeling and Analysis in MATLAB and Simulink.[online]{Available}: http://www.mathworks.com/videos/electrical-distribution-system-modeling-and-analysis-in-matlab-and-Simulink-81978.html

[42] M.Panwar, S. Suryanarayanan, S. Chakraborty, "Steady-state modeling and simulation of a distribution feeder with distributed energy resources in a real-time digital simulation envi-

ronment," in *North American Power Symposium (NAPS)*, 2014, vol., no., pp.1-6, 7-9 Sept. 2014

[43] J. Blanger, J. N. Paquin and P. Venne "The What, Where and Why of Real-Time Simulation", in *IEEE PES General Meeting, Minneapolis*, USA (July 25-29, 2010)

[44] Teninge, A.; Besanger, Y.; Colas, F.; Fakham, H.; Guillaud, X.,"Real-time simulation of a medium scale distribution network: Decoupling method for multi-CPU computation", *Complexity in Engineering (COMPENG)*, 2012 , vol., no., pp.1,6, 11-13 June 2012

[45] MathWorks. Average Model of a 100-kW Grid-Connected PV Array [Online].{Available}:http://www.mathworks.com/help/physmod/sps/examples/average-model-of-a-100-kw-grid-connected-pv-array.html

[46] Moacyr A. G. de Brito, Leonardo P. Sampaio, Luigi G. Jr., Guilherme A. e Melo, Carlos A. Canesin "Comparative Analysis of MPPT Techniques for PV Applications", 2011 *International Conference on Clean Electrical Power (ICCEP)*.

[47] B. Bahrani.; A. Karimi; B. Rey; A. Rufer, "Decoupled dq-Current Control of Grid-Tied Voltage Source Converters Using Nonparametric Models," in*Industrial Electronics, IEEE Transactions* on, vol.60, no.4, pp.1356-1366, April 2013

[48] K.E.,Yeager; J.R.,Willis, "Modeling of emergency diesel generators in an 800 megawatt nuclear power plant," in *Energy Conversion, IEEE Transactions* on , vol.8, no.3, pp.433-441, Sep 1993

[49] MathWorks. Emergency Diesel-Generator and Asynchronous Motor [online]{Available}http://www.mathworks.com/help/physmod/sps/examples/emergency-diesel-generator-and-asynchronous-motor.html

[50] IEEE: “EEE 1547-2003: IEEE Standard for Interconnecting DistributedResources with Electric Power Systems.” 2003.

[51] S. Chowdhury, S.P. Chowdhury, P. Crossley Microgrids and active distribution networks, IET renewable energy series 6 IET, London (2009)

[52] MathWorks. Battery. Implement generic battery mode. [online]{Available}:http://www.mathworks.com /help/physmod/sps/powersys/ref/battery.html

[53] Technical Requirement for connecting distributed resources to Manitabo Hydro System, DRG 2003, Rev2, MBHydro Electric Board; 2010

Appendix A

SIMULATION RESULTS, MATLAB™ CODES, AND FILES

A.1 SIMULINK™ AND RT-LAB™ VERSIONS

```
--------------------------------------------------------------------------------
MATLAB Version 7.13.0.564 (R2011b)
MATLAB License Number: 334870
Operating System: Microsoft Windows 7 Version 6.1 (Build 7601: Service Pack 1)
Java VM Version: Java 1.6.0_17-b04 with Sun Microsystems Inc.
Java HotSpot(TM) Client VM mixed mode
--------------------------------------------------------------------------------
MATLAB                                                  Version 7.13       (R2011b)
Simulink                                                Version 7.8        (R2011b)
ARTEMIS Blockset                                        Version 7.0.1.736    (R2011b)
Communications System Toolbox                           Version 5.1        (R2011b)
Computer Vision System Toolbox                          Version 4.1        (R2011b)
Control System Toolbox                                  Version 9.2        (R2011b)
Curve Fitting Toolbox                                   Version 3.2        (R2011b)
DSP System Toolbox                                      Version 8.1        (R2011b)
Data Acquisition Toolbox                                Version 3.0        (R2011b)
Embedded Coder                                          Version 6.1        (R2011b)
Fixed-Point Toolbox                                     Version 3.4        (R2011b)
Fuzzy Logic Toolbox                                     Version 2.2.14     (R2011b)
Global Optimization Toolbox                             Version 3.2        (R2011b)
Image Acquisition Toolbox                               Version 4.2        (R2011b)
Image Processing Toolbox                                Version 7.3        (R2011b)
Instrument Control Toolbox                              Version 3.0        (R2011b)
MATLAB Builder EX                                       Version 2.1        (R2011b)
MATLAB Coder                                            Version 2.1        (R2011b)
```

```
MATLAB Compiler                                  Version 4.16       (R2011b)
MATLAB Report Generator                          Version 3.11       (R2011b)
Mapping Toolbox                                  Version 3.4        (R2011b)
Model Predictive Control Toolbox                 Version 4.0        (R2011b)
Neural Network Toolbox                           Version 7.0.2      (R2011b)
Optimization Toolbox                             Version 6.1        (R2011b)
Parallel Computing Toolbox                       Version 5.2        (R2011b)
Partial Differential Equation Toolbox            Version 1.0.19     (R2011b)
RT-EVENTS Blockset                               Version 4.0.0.433  (R2011B.x)
RT-LAB                                           Version v10.5.9.356 (R2011b.x)
RT-XSG                                           Version v2.3.1.135sgUnsupported(Rx.x)
Robust Control Toolbox                           Version 4.0        (R2011b)
Signal Processing Toolbox                        Version 6.16       (R2011b)
SimBiology                                       Version 4.0        (R2011b)
SimDriveline                                     Version 2.1        (R2011b)
SimElectronics                                   Version 2.0        (R2011b)
SimEvents                                        Version 4.0        (R2011b)
SimMechanics                                     Version 3.2.3      (R2011b)
SimPowerSystems                                  Version 5.5        (R2011b)
Simscape                                         Version 3.6        (R2011b)
Simulink Coder                                   Version 8.1        (R2011b)
Simulink Control Design                          Version 3.4        (R2011b)
Simulink Design Optimization                     Version 2.0        (R2011b)
Spreadsheet Link EX                              Version 3.1.4      (R2011b)
Stateflow                                        Version 7.8        (R2011b)
Statistics Toolbox                               Version 7.6        (R2011b)
Symbolic Math Toolbox                            Version 5.7        (R2011b)
System Identification Toolbox                    Version 7.4.3      (R2011b)
Wavelet Toolbox                                  Version 4.8        (R2011b)
```

A.2 MATLAB™ CODE FOR THE IEEE 13-NODE LINE PARAMETERS

```
Ts=50e-6;
Rm=1e3;
Rm1=1e6;
%IEEE 13-Node test feeder impedances

% miles/km
mi2km = 1.609344;

% feet to km
ft2km = 0.0003048;

% microsiemens to Farads
ms2F = 1/2/pi/60*1e-6;



%configuration 601
R_config_601= [
0.3465    0.1560    0.1580
   0.1560     0.3375   0.1535
   0.1580      0.1535     0.3414  ];

X_config_601 =  [
 1.0179     0.5017     0.4236
   0.5017       1.0478      0.3849
```

```
   0.4236          0.3849      1.0348 ];

B_config_601=[
6.2998   -1.9958   -1.2595
  -1.9958      5.9597   -0.7417
  -1.2595        -0.7417     5.6386];


R_601 = R_config_601/mi2km;

L_601 = X_config_601/mi2km/2/pi/60;

C_601 = B_config_601/mi2km*ms2F;




%configuration 602

R_config_602=[
0.7526     0.1580     0.1560
  0.1580       0.7475      0.1535
  0.1560         0.1535         0.7436  ];

 X_config_602= [
 1.1814     0.4236     0.5017
       0.4236       1.1983    0.3849
       0.5017         0.3849   1.2112];

B_config_602=[
           5.6990   -1.0817   -1.6905
```

```
              -1.0817      5.1795   -0.6588
              -1.605           -0.6588    5.4246];

R_602 = R_config_602/mi2km;

L_602 = X_config_602/mi2km/2/pi/60;

C_602 = B_config_602/mi2km*ms2F;


%configuration 603

R_config_603=[
    1.3294    0.2066
              0.2066       1.3238  ];

X_config_603= [

  1.3471    0.4591
       0.4591    1.3569];

B_config_603=[
               4.7097   -0.8999
                    -0.8999    4.6658];

R_603 = R_config_603/mi2km;

L_603 = X_config_603/mi2km/2/pi/60;

C_603 = B_config_603/mi2km*ms2F;
```

```
%configuration 604
R_config_604=[
 1.3238       0.2066

   0.2066               1.3294  ];


X_config_604=[
  1.3569       0.4591

   0.4591              1.3471];

B_config_604=[
            4.6658      -0.8999

               -0.8999         4.7097];


R_604 = R_config_604/mi2km;

L_604 = X_config_604/mi2km/2/pi/60;

C_604 = B_config_604/mi2km*ms2F;


%configuration 605
R_config_605=[

   1.3292 ];

X_config_605 = [
```

```
    1.3475];


B_config_605=[
               4.5193];


R_605 = R_config_605/mi2km;

L_605 = X_config_605/mi2km/2/pi/60;

C_605 = B_config_605/mi2km*ms2F;



%configuration 606

R_config_606=[
0.7982   0.3192    0.2849
  0.3192           0.7891   0.3192
  0.2849            0.3192      0.7982 ];

X_config_606=[
 0.4463     0.0328    -0.0143
       0.0328        0.4041     0.0328
       -0.0143      0.0328      0.4463];

B_config_606=[
          96.8897    0.0000    0.0000
            0        96.8897    0.0000
```

```
            0            0      96.8897];

R_606 = R_config_606/mi2km;

L_606 = X_config_606/mi2km/2/pi/60;

C_606 = B_config_606/mi2km*ms2F;



%configuration 607

R_config_607=[
 1.3425     ];

X_config_607=[
  0.5124    ];
B_config_607=[
           88.9912   ];

R_607 = R_config_607/mi2km;

L_607 = X_config_607/mi2km/2/pi/60;

C_607 = B_config_607/mi2km*ms2F;
```

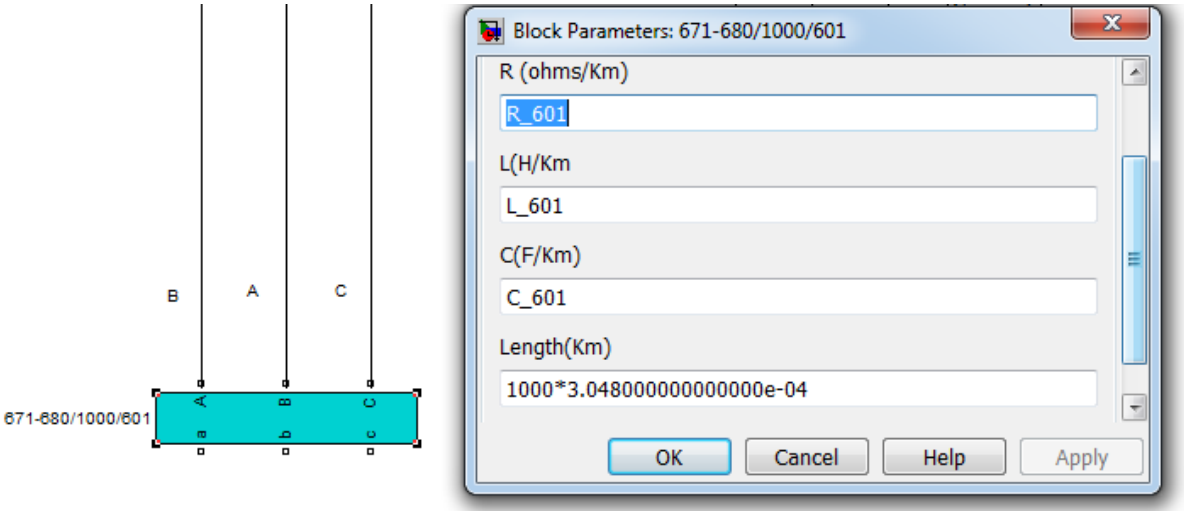

Figure A.1: Line parameters in Simulink™ block.

The values calculated from this script are used in the line model as shown Figure A.1

A.3 PROCEDURE TO CHANGE TAPS IN SIMULINK™ OLTC MODEL

```
The following procedure explains how to increase the number of taps from 8
(17 OLTC positions)
 to 10 (21 OLTC positions)
 If you want to decrease the number of taps, follow the reverse procedure
(Change 'add' to ' cut' and skip step C3).

A) Open the Three-Phase OLTC Transformer mask (use Edit/Edit mask)
  In Initialization section, modify 1st line as below:
         NumberOfTaps=10;

B) Open the TransformerA block dialog box inside the Three-Phase OLTC Transformer
(use Edit/Look under mask)
  and change the 'Number of Taps' parameter from 7 to 9
(adding two intermediate taps on upper left winding (winding 1)).

C) Open the OLTCA block inside the Three-Phase OLTC Transformer
 (use Edit/Look under mask) and make the following changes:
   1) Open the dialog box of the Demux block and change the parameter
```

'Number of outputs' from 9 to 11.

2) Add 2 switches labeled Sw9 and Sw10 (duplicate Sw8 block); Position these two blocks on top of Sw8 block.

3) Open the dialog box of Sw9 and Sw10 blocks and change the parameter "Initial state" as follows:

Sw9 --> InitialState(10)

Sw10-->InitialState(11)

4) Add two connection ports labeled respectively Tap9 and Tap10 (duplicate Tap8 block). Position these two blocks on top of Tap8 block.

5) Renumber ALL connection ports as follows:

Open dialog box of each connection port and change 'Port number' and 'Port location' parameters as in the table below.

(all port locations should be set to 'right' except for 'Out' port which must be 'left')

Start the renumbering with the top port labeled Tap10.

Port label	Port number	Port location
Tap10	1	right
Tap9	2	right
.....	.....	.....
Tap 1	11	right
Tap 0	12	right
W2+	13	right
Out	14	left

6) Connect terminal 1 of Sw9 and Sw10 respectively to ports labeled Tap10 (port #1) and Tap9 (port #2)

7) Connect terminal 2 of Sw9 and Sw10 respectively to nodes labeled R2 and R1

8) Close the OLTCA block.

D) Connect the Tap10, Tap9 ...Tap0 connectors of OLTCA respectively to 1+, 1.1, ... 1 connectors of tapped winding of TransformerA.

E) Cut the OLTCB and OLTCC blocks and replace them with a duplicate of OLTCA block. Rename these two blocks OLTCB and OLTCC.

F) Cut the TransformerB and TransformerC blocks and replace them with a duplicate of TransformerA block. Rename these two blocks TransformerB and TransformerC.

G) Make connections between OLTC to Transformer for phases B and C as for phase A.

H)Ckeckthat the secondary windings of the three transformers are connected in Delta (D1)

A.4 MATLAB™ CODE FOR ZERO CROSSING AND COUNTER

```
function T = fcn(u,v)
j = 0;
if j==0
    T =0;
    j=1;
end
if v ≥ 0  && u ≤0 %sign change form +ve to -ve
   T = 1; %recording the time instant
end
```

```
function count = fcn(rst,a)
if rst == 1
    count=1;
else
count =a+1;
end
```

A.5 CONTROLLED CURRENT SOURCE IN THE DISTRIBUTION MODEL

Table A.1: Controlled current source in 13-Node distribution model (1000MVA transformer)

Transformer : Pn =1000e6 VA 480/120-120 winding: 240 rms R2 pu : 0.0 L2 pu 0.0 winding: 120 rms R2 pu : 0.011 L2 pu 0.02 winding: 120 rms R2 pu : 0.011 L2 pu 0.02							
pu_240 (V)	pu_120 (V)	pu_120 (V)	P (W)	Q (Vars)	S = sqrt($P^2 + Q^2$)	current =S/V (A)	current (A) 120V side
1.019	1.019	1.019	10220	-6700	12220	100	100
1.018	1.018	1.018	20470	-13370	24449	200	200
1.018	1.018	1.018	51310	-33160	61093	500	500
1.018	1.018	1.018	103100	-65450	122120	1000	1000
1.02	1.02	1.02	315700	-187400	367131	2999	3000
1.025	1.025	1.025	1121000	-508500	1230940	10008	10000
Transformer : Pn =500e6 VA 480/120-120 winding: 240 rms R2 pu : 0.0 L2 pu 0.0 winding: 120 rms R2 pu : 0.011 L2 pu 0.02 winding: 120 rms R2 pu : 0.011 L2 pu 0.02							
pu_240 (V)	pu_120 (V)	pu_120 (V)	P (W)	Q (Vars)	S = sqrt($P^2 + Q^2$)	current =S/V (A)	current (A) 120V side
1.017	1.017	1.017	10190	-6705	12198	100	100
1.017	1.017	1.017	20400	-13370	24391	200	200
1.016	1.016	1.016	51170	-33150	60970	500	500
1.016	1.016	1.016	82110	-52590	97508	800	800
1.016	1.016	1.016	102800	-65370	121824	999	1000
1.015	1.015	1.015	207700	-127000	243451	1999	2000
pu_240 (V)	pu_120 (V)	pu_120 (V)	P (W)	Q (Vars)	S = sqrt($P^2 + Q^2$)	current =S/V (A)	current (A) 120V side
1.017	1.017	1.017	-10170	6742	12202	100	100
1.021	1.021	1.021	-30610	20340	36752	300	300
1.022	1.022	1.022	-81230	54980	98087	800	800
1.023	1.023	1.023	-151200	105100	184140	1500	1500
1.025	1.026	1.026	-297800	218500	369360	3000	3000
1.032	1.034	1.034	-577200	470600	744731	6002	6000

Table A.2: Controlled current source in 13-Node distribution model (500MVA transformer)

Transformer : Pn =500e6 VA 480/120-120 winding: 240 rms R2 pu : 0.0 L2 pu 0.0 winding: 120 rms R2 pu : 0.011 L2 pu 0.02 winding: 120 rms R2 pu : 0.011 L2 pu 0.02									
pu_240 (V)	pu_120 (V)	pu_120 (V)	P (W)	Q (Vars)	S = sqrt($P^2 + Q^2$)	current =S/V (A)	current (A) 120V side	Single winding	current in secondary (A)
1.021	1.021	1.021	12260	116	12261	100	100	50	100
1.023	1.023	1.023	36840	350	36842	300	300	150	300
1.028	1.028	1.028	98680	937	98684	800	800	400	800
1.029	1.031	1.031	148500	1411	148507	1200	1200	600	1200
1.035	1.038	1.038	249200	1000	249202	2001	2000	1000	2000
1.049	1.054	1.054	506300	4810	506323	4003	4000	2001	4002
1.062	1.07	1.07	770500	7322	770535	6001	6000	3000	6000
1.077	1.088	1.088	1045000	9933	1045047	8004	8000	4001	8002
1.083	1.095	1.095	1183000	11250	1183053	9003	9000	4501	9002
1.086	1.095	1.095	1252000	11910	1252057	9529	9500	4751	9502

A.6 OPAL-RT™ AND RT-LAB™ ISSUES, CHALLENGES AND SOLUTIONS

1. Check the MATLAB™ compatibility : 32bit or 64bit
2. Check the current target is set as : development node
3. Opcomm block is present , also every system must have master and console block.
4. RT lab modules in Simulink™ library are accessible only when MATLAB™ opened through RT-Lab
5. The data should be saved in order to observe the proper waveforms.
6. In order to reduce the computation the master and slave system should have no scopes and displays.
7. One good practice is to run the simulation offline on Simulink™ before building the model. This would help identify any error in the model before compiling in RT-LAB
8. The powergui block should be placed in top level of the system

A.7 SIMULINK™ MODELS AND FILES

Table A.3: RT-LAB™ and Simulink™ models

File name	Description
CSU_LDRD_20151006_IEEE_13node.mdl	This model contains the OPAL-RT™ compatible IEEE 13-Node distribution system
CSU_LDRD_20151006_IEEE_13node_sim.mdl	This model contains the Simulink™ only compatible IEEE 13-Node distribution system
CSU_LDRD_20151006_analog_IO_protection.mdl	Contains the 13-Node distribution system with split phase 240/120V transformer driving a analog I/O with protection block for frequency and voltage
CSU_LDRD_20151006_microgrid.mdl	Contains the 13-Node distribution system, PV array model, diesel generator with synchronization switch-control and lead acid battery model.
init_PV.m	Used to load the PV data in the PV cell; change this data to change the characteristics of the PV panel.
IEEE_config_line_test.m	Contains the line parameters for the PI line model

Note: See the Matlab/Simulink™ and RT-LAB™ versions for compatibility, given in appendix-A.1.